NASA TECHNICAL NOTE

NASA TN D-5375

c. 1

NASA TN D-5375

EFFECT OF INJECTION ELEMENT RADIAL DISTRIBUTION AND CHAMBER GEOMETRY ON ACOUSTIC-MODE INSTABILITY IN A HYDROGEN OXYGEN ROCKET

by John P. Wanhainen and C. Joe Morgan

Lewis Research Center
Cleveland, Ohio

NATIONAL AERONAUTICS AND SPACE ADMINISTRATION • WASHINGTON, D. C. • AUGUST 1969

EFFECT OF INJECTION ELEMENT RADIAL DISTRIBUTION AND CHAMBER GEOMETRY ON ACOUSTIC-MODE INSTABILITY IN A HYDROGEN OXYGEN ROCKET

By John P. Wanhainen and C. Joe Morgan

Lewis Research Center
Cleveland, Ohio

NATIONAL AERONAUTICS AND SPACE ADMINISTRATION

For sale by the Clearinghouse for Federal Scientific and Technical Information
Springfield, Virginia 22151 – CFSTI price $3.00

ABSTRACT

An experimental investigation of both 20 000- and 50 000-pound- (89- and 222-kN) thrust engines with concentric tube injectors was conducted to determine the effect of variations in injection element radial distribution, thrust chamber diameter and thrust chamber axial flow area on tangential-acoustic-mode stability characteristics. These characteristics were evaluated by determining the hydrogen injection temperature below which combustion was unstable. An annulus, void of injection elements, at the perimeter of the injector, was found to be detrimental to stability. A generalized response factor model was used in the analysis of the experimental results.

EFFECT OF INJECTION ELEMENT RADIAL DISTRIBUTION AND CHAMBER GEOMETRY ON ACOUSTIC-MODE INSTABILITY IN A HYDROGEN OXYGEN ROCKET

by John P. Wanhainen and C. Joe Morgan

Lewis Research Center

SUMMARY

An experimental investigation was conducted at the Lewis Research Center to determine the effect of variations in (1) radial distribution of injection elements, (2) thrust chamber diameter, and (3) thrust chamber axial flow area on combustion stability characteristics of hydrogen-oxygen rocket engines. The experiments were performed in both 20 000- and 50 000-pound- (89- and 222-kN-) thrust engines using concentric tube injectors operating at a chamber pressure of 300 psia (2068 kN/m^2 abs). The stability of each configuration was evaluated by ramping the hydrogen injection temperature downward until combustion became unstable.

An annulus, void of injection elements, at the perimeter of the injector was found to be detrimental to the tangential-mode stability characteristics of the combustor. The destabilizing effect of the annulus appeared to be independent of thrust chamber diameter and the number of injection elements. Inserting a partial length sleeve of 4 inches (10.16 cm) into the annulus provided the same stability as the full-length chamber. The length of the sleeve could be related to the length of the combustion zone.

A generalized response factor model was used in the analysis of the experimental results. The oxygen response was assumed to be atomization controlled. For the model, a correlation equation was derived to calculate oxygen jet breakup time. This equation compared well qualitatively with a published empirical equation but it was not quantitatively exact for stability prediction.

INTRODUCTION

An important aspect of liquid rocket engine design is the stability of the combustion process, particularly its stability with respect to destructive acoustic modes. To date, the development of rocket engines with a reasonable stability margin has been largely through a "cut and try" process. Cost increases and time delays due to such development methods have been formidable. In an attempt to alleviate this problem, an extensive program to study combustion instability in engines using hydrogen-oxygen propellants and earth-storable propellants was initiated at the Lewis Research Center. Emphasis was placed on the tangential mode of instability which is frequently encountered and difficult to eliminate in large rocket development programs.

In a previous investigation with hydrogen-oxygen propellants (ref. 1), the effect of varying propellant injection velocity on acoustic mode instability was determined. From that study, a rating technique for combustion stability and a correlation of the stability limits was developed. Subsequently, an empirical correlation was developed which permitted prediction of the change in stable operating limits for several geometric and operating variables (ref. 2). The purpose of the experiments reported herein was to check the applicability of the previous results to varying chamber and injector design geometry. Specifically, the effects of changes in chamber diameter and radial distribution of injection elements on stability are presented in this report. The stability data are analyzed using a generalized response factor model.

The investigation was conducted in the Rocket Engine Test Facility using hydrogen-oxygen rocket engines which produced 20 000 and 50 000 pounds (89 and 222 kN) of thrust at a chamber pressure of 300 psia (2068 kN/m^2 abs). The oxidant-fuel ratio was varied from 4 to 6.5. Concentric tube injection elements were used in heat-sink combustion hardware. Variables in the experimental program using 397-element injectors included (1) radial distribution of injection elements, (2) chamber diameter, and (3) chamber axial flow area. A limited number of additional tests were made with injectors differing in the number of injection elements.

The stability characteristics of the various configurations were evaluated by ramping the hydrogen injection temperature down to determine the transition temperature at the point of instability. In addition to the stability data, the performance of the various engine configurations is tabulated.

APPARATUS

Test Facility

The Rocket Engine Test Facility of the Lewis Research Center is a 50 000-pound- (222.4-kN-) thrust sea level stand equipped with an exhaust gas muffler and scrubber. Sketches of the facility and a detailed description may be found in reference 1.

Engine

The basic engine which is shown in figure 1, included an injector, a cylindrical heat-sink thrust chamber and a convergent-divergent exhaust nozzle with a contraction ratio of 1.9 and an expansion ratio of 1.3. (The expansion ratio was selected for operating convenience, and it had no effect on the combustion process.) Dimensions of the basic engine, along with other variations in thrust chamber and nozzle geometry used in this investigation, are shown in table I. A total of eight different cylindrical thrust chambers which varied in diameter from 8.35 to 18.5 inches (21.21 to 47 cm) were used in the investigation. Other combustors which were used to evaluate the effect of changes in axial flow area included four configurations with cylindrical sleeves (configurations T, U, V, W of table I), one configuration with a tapered sleeve (X), and one configuration with a spiral sleeve (Y). The internal radius of the spiral sleeve varied from 4.18 to 5.39 inches (10.6 to 13.7 cm). The inner surfaces of the heat-sink combustion chamber and nozzle were coated with 0.030-inch- (0.0762-cm-) thick layer of flame-sprayed zirconium oxide to reduce the rate of heat transfer into the metal. This allowed a test duration of 3 seconds which was adequate to obtain the test results.

Concentric tube elements, consisting of a central oxidizer tube surrounded by a concentric fuel annulus, were used in the investigation. Cross-sectional views of the elements used in the 421-, 397-, 201-, and 157-element injectors are shown in figure 2.

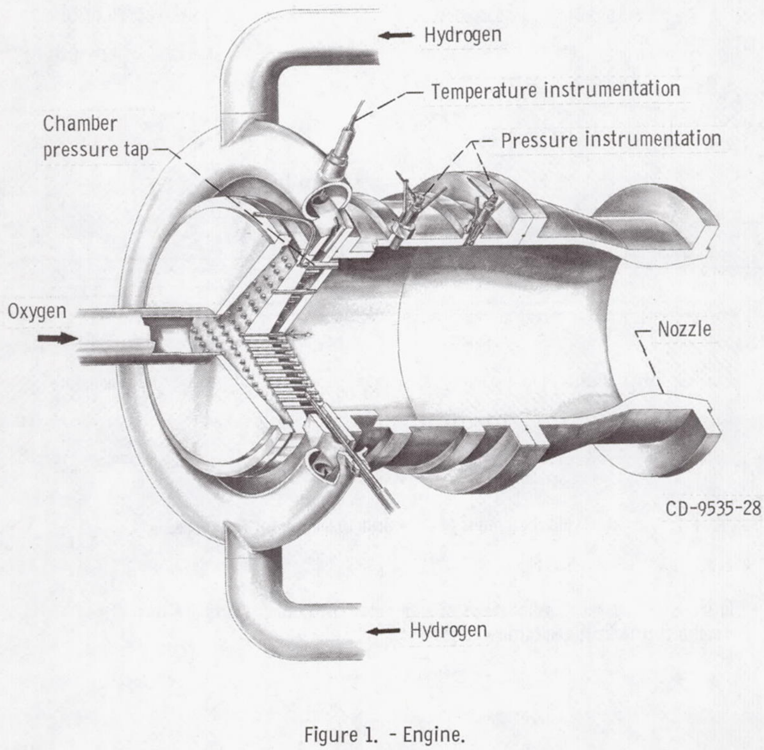

Figure 1. - Engine.

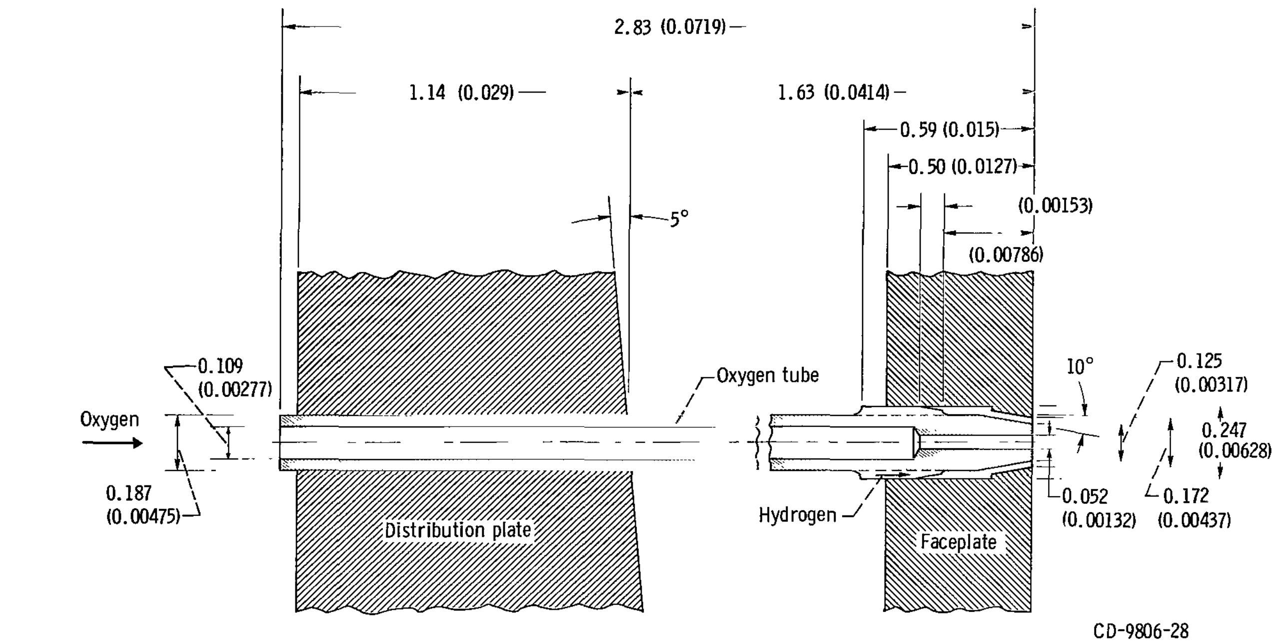

(a) Typical element of 397- and 421-element injectors.

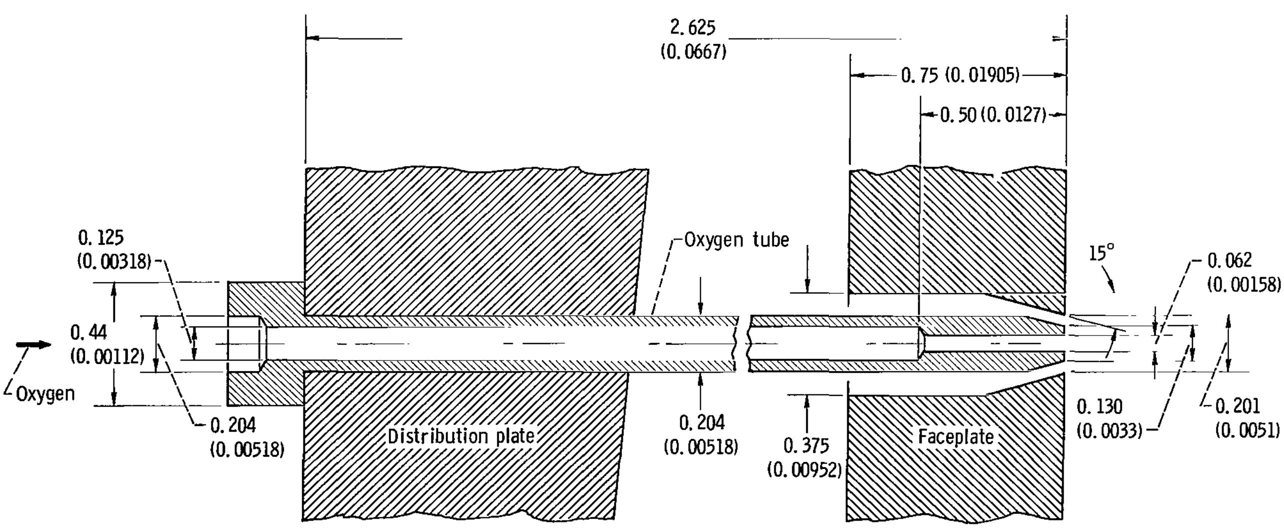

(b) Typical element of 201- and 157-element injectors.

CD-10416-28

Figure 2. - Cross-sectional views of elements. (All dimensions are in inches (meters) unless noted otherwise.)

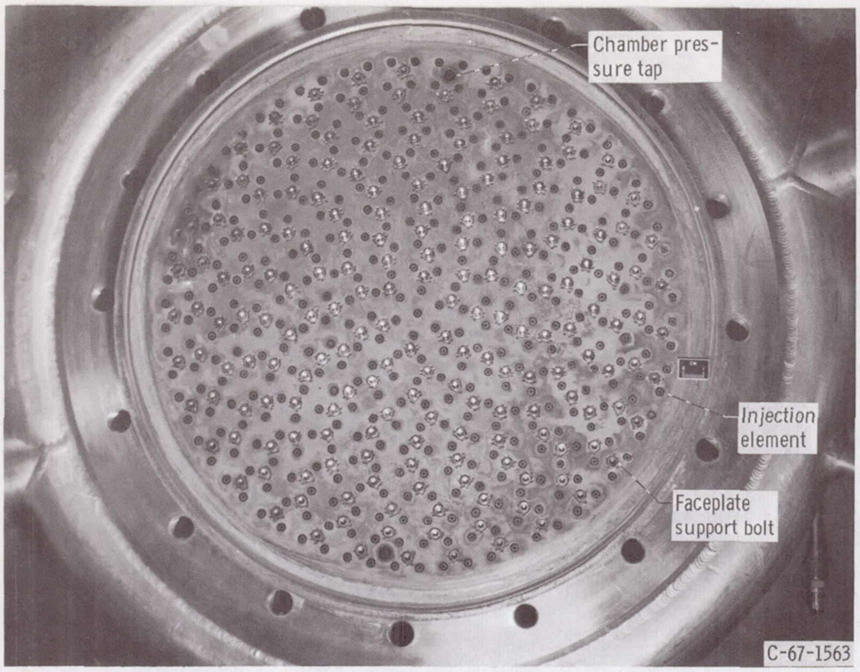

(a) 397-Element, 100 percent radial distribution in 10.78-inch- (27.38-cm-) diameter thrust chamber. Element circle spacing, 0.468 inch (1.19 cm).

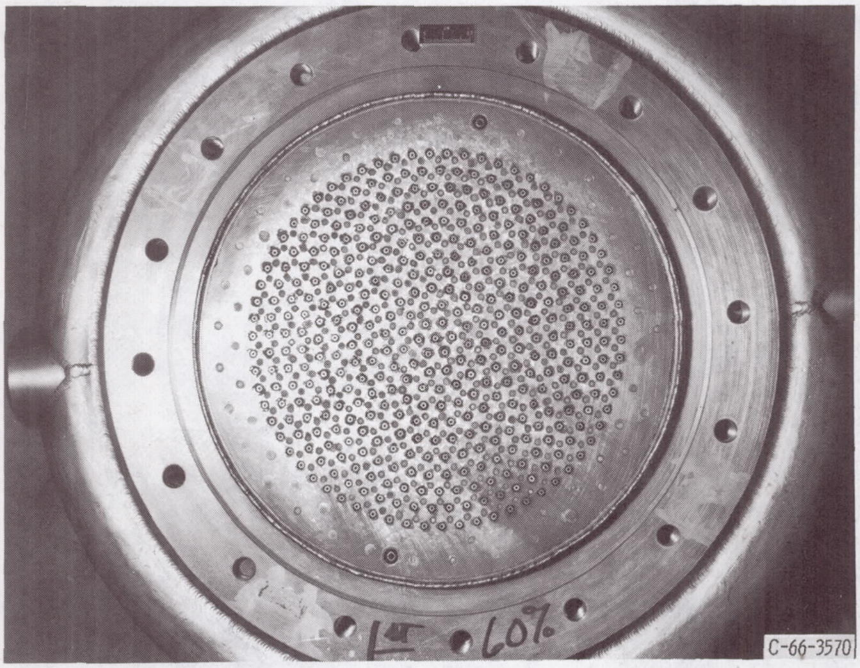

(b) 397-Element, 60 percent radial distribution in 10.78-inch- (27.38-cm-) diameter thrust chamber. Element circle spacing, 0.362 inch (0.92 cm).

Figure 3. - Faceplate view of concentric tube injectors.

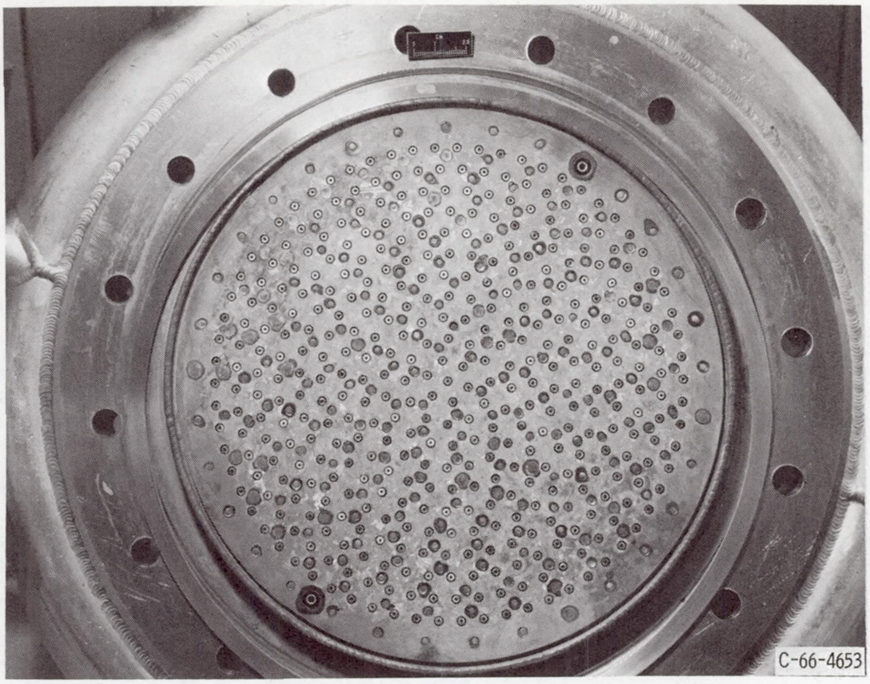

(c) 397-Element, 72 percent radial distribution in 10.78-inch- (27.38-cm-) diameter thrust chamber. Element circle spacing, 0.398 inch (1.012 cm).

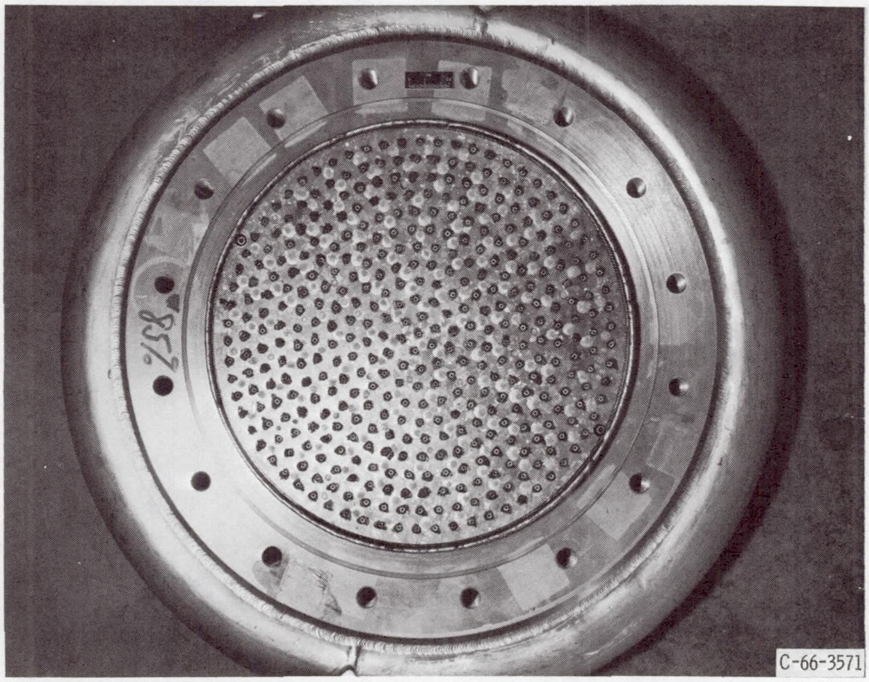

(d) 397-Element, 85 percent radial distribution in 10.78-inch- (27.38-cm-) diameter thrust chamber. Element circle spacing, 0.432 inch (1.098 cm).

Figure 3. - Continued.

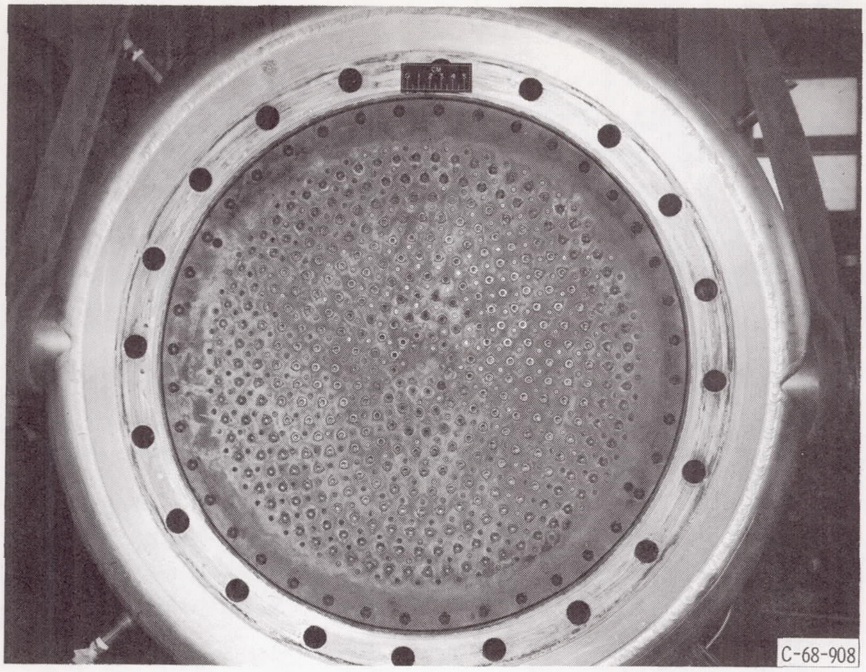

(e) 397-Element, 100 percent radial distribution in 15.7-inch- (29.88-cm-) diameter thrust chamber. Element circle spacing, 0.683 inch (1.735 cm).

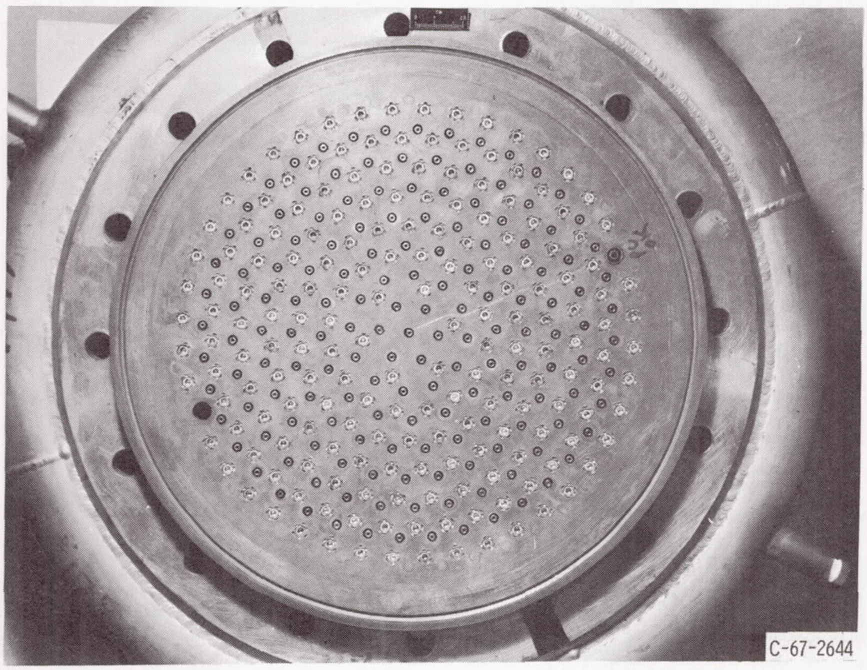

(f) 201-Element, 85 percent radial distribution in 10.78-inch- (27.38-cm-) diameter thrust chamber.

Figure 3. - Continued.

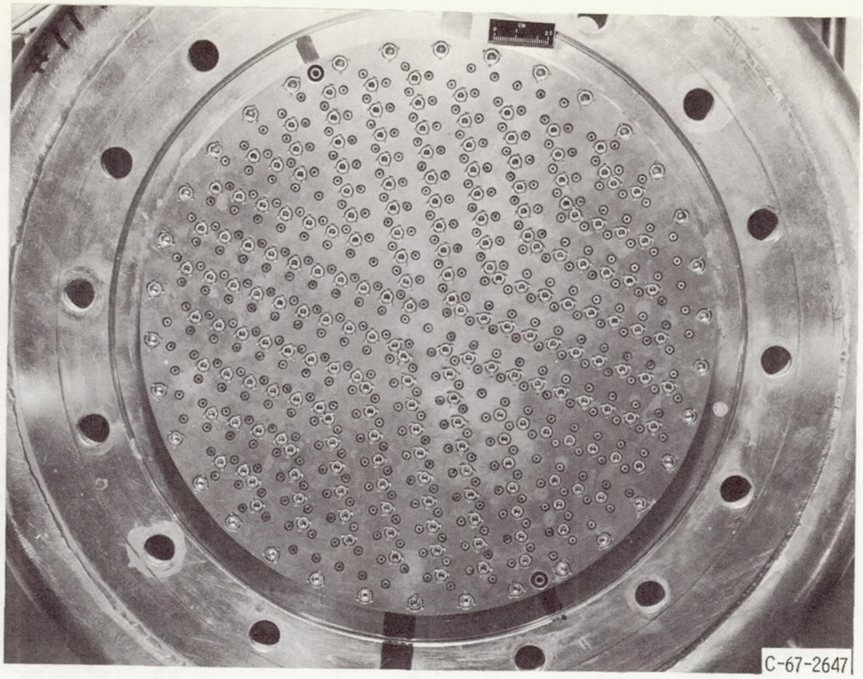

(g) 421-Element, 85 percent radial distribution in 10.78-inch- (27.38-cm-) diameter thrust chamber.

Figure 3. - Concluded.

The 421- and the 397-element injectors used the element shown in figure 2(a). The 201- and the 157-element injectors used the element shown in figure 2(b). In the course of the test program, the injection orifices of the 397-element injector with an element concentric circle spacing of 0.683 inch (1.735 cm) were resized for the higher weight flows corresponding to the 50 000-pound- (222-kN-) thrust operating condition. The oxygen orifice was increased from 0.052 to 0.081 inch (0.0132 to 0.0206 cm), and the hydrogen orifice was increased from 0.172 to 0.204 inch (0.0437 to 0.0518 cm).

The faceplate view of the 10.78-inch- (27.38-cm-) diameter injector with uniform distribution of elements is shown in figure 3(a). The injector had 397 elements arranged uniformly in 11 concentric, equally spaced circles. The spacing of the element circles was 0.468 inch (1.189 cm). The faceplate was fabricated from 0.5-inch- (1.27-cm-) thick oxygen-free copper which has good heat-sink capability and good thermal conductivity. Faceplate views of other 397-element injectors with element circle spacings of 0.362, 0.398, 0.432, and 0.683 inch (0.92, 1.012, 1.098, and 1.735 cm) are shown in figures 3(b), (c), (d), and (e), respectively. With the exception of the element pattern, the injectors were the same in all respects (i.e., same elements, impingement angle, and faceplate thickness). The element distribution which is listed in table I for each combustor was defined as the ratio of the active face area to the thrust chamber cross-sectional area. The active face area was arbitrarily defined as the area within a circle

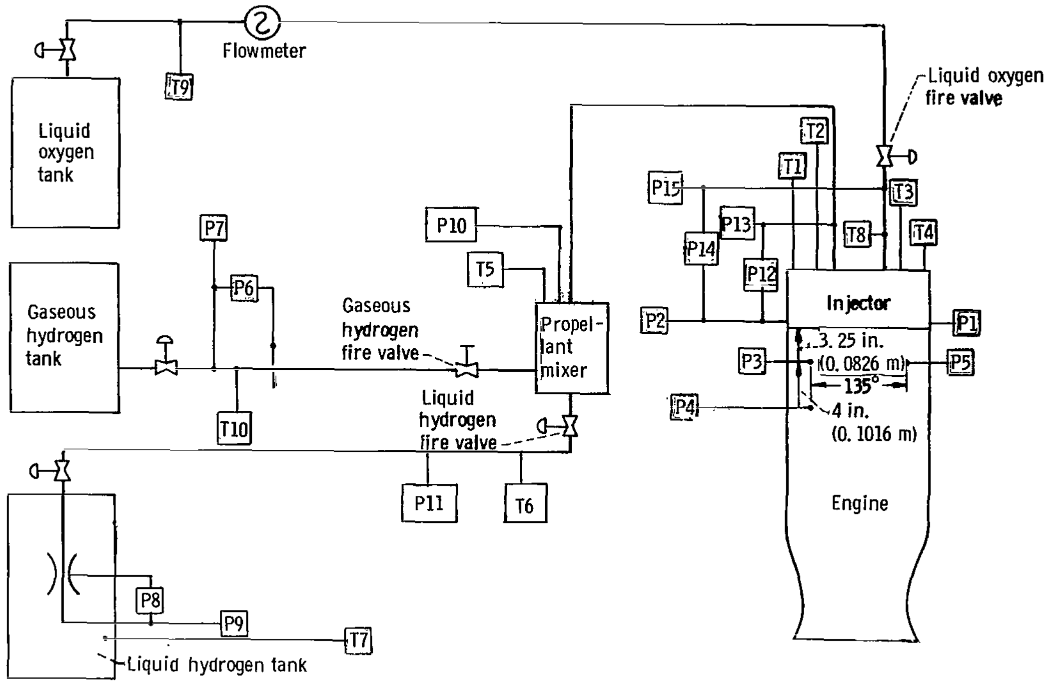

P1	Static chamber pressure (injector face), four-arm strain-gage transducer 1
P2	Static chamber pressure (injector face), four-arm strain-gage transducer 2
P3	Dynamic chamber pressure, water-cooled quartz pressure transducer 3
P4	Dynamic chamber pressure, water-cooled quartz pressure transducer 4
P5	Dynamic chamber pressure, water-cooled quartz pressure transducer 5
P6	Gaseous hydrogen orifice differential pressure, four-arm strain-gage transducer
P7	Gaseous hydrogen orifice pressure, four-arm strain-gage transducer
P8	Liquid hydrogen venturi differential pressure, four-arm strain-gage type
P9	Liquid hydrogen venturi pressure, four-arm strain-gage transducer
P10	Hydrogen mixer pressure, four-arm strain-gage transducer
P11	Liquid hydrogen line pressure, four-arm strain gage transducer
P12	Hydrogen injection differential pressure, four-arm strain-gage transducer
P13	Hydrogen injection pressure, four-arm strain-gage transducer
P14	Oxygen injection differential pressure, four-arm strain-gage transducer
P15	Oxygen injection pressure, four-arm strain-gage transducer
T1	Hydrogen injector temperature, carbon resistor sensor probe 1
T2	Hydrogen injector temperature, carbon resistor sensor probe 2
T3	Hydrogen injector temperature, carbon resistor sensor probe 3
T4	Hydrogen injector temperature, carbon resistor sensor probe 4
T5	Hydrogen mixer temperature, carbon resistor sensor probe
T6	Liquid hydrogen line temperature, carbon resistor sensor probe
T7	Liquid hydrogen venturi temperature, platinum type
T8	Oxygen injection temperature, copper-constantan thermocouple
T9	Oxygen flowmeter temperature, platinum type
T10	Gaseous hydrogen orifice temperature, iron-constantan thermocouple

Figure 4. - Test instrumentation and transducer locations.

whose diameter was equal to the diameter of the outer row of elements plus the element circle spacing.

Other injectors with 201 and 421 injection elements used in the test program are shown in figures 3(f) and (g). Both injectors also utilized oxygen-free, copper heat-sink faceplates. In the course of the test program, the 201-element injector was reduced to 157 elements by closing off the outer row of elements. In a 10.78-inch- (27.38-cm-) diameter thrust chamber, this modification resulted in a change in the element distribution from 100 to 72 percent.

Instrumentation

The instrumentation used in the investigation and locations for the various transducers are shown on a schematic diagram of the engine and associated plumbing in figure 4. Piezoelectric, water-cooled, flush-mounted pressure transducers were used at three locations on the thrust chamber wall (fig. 4) to determine the amplitude and phase

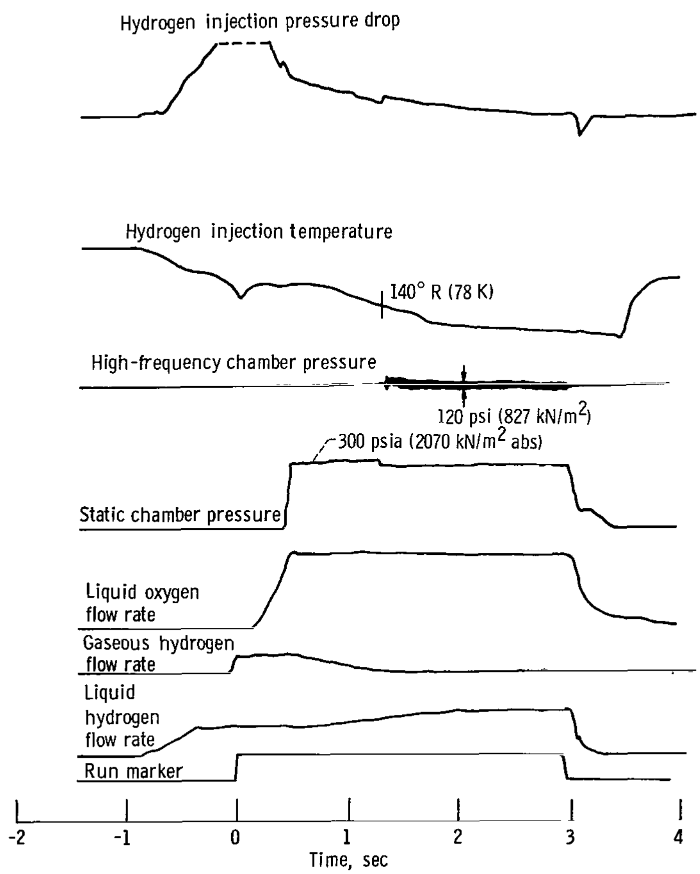

Figure 5. - Oscillograph traces of typical screech test illustrating hydrogen temperature rating technique.

relations of the pressure field for identification of the screech mode. The amplitude response of the chamber transducers as installed was flat to within 10 percent to a frequency of 10 000 hertz and had a nominal resonant frequency of 20 000 hertz. The signals from high-frequency response transducers were recorded on magnetic tape as well as on direct reading oscillographs for visual monitoring during the tests. The accuracy of the performance data is estimated to be ±2 percent.

PROCEDURE

The effect of changes in element radial distribution and thrust chamber geometry was evaluated by comparing the hydrogen temperature stable operating limits. A typical oscillograph record of a test to determine the stable operating limits of a combustor in terms of hydrogen injection temperature is presented in figure 5. The hydrogen temperature ramp was accomplished by starting the run on a mixture of liquid hydrogen and warm gaseous hydrogen and then reducing the percentage of gas introduced in a predetermined ramp while simultaneously opening the liquid hydrogen valve to maintain a constant total flow. Mixing was accomplished by swirling the liquid into the gaseous hydrogen stream. (A detailed description of the hydrogen temperature controller may be found in ref. 1.) The operating parameters of chamber pressure, oxidant-fuel ratio, and hydrogen injection temperature at the onset of instability were recorded and are presented in table II. The time of transition into instability was indicated by an oscillograph trace of a high-frequency pressure transducer. Combustion was considered unstable when a periodic wave-form reached an amplitude of 10 to 15 psi (69 to 104 kN/m^2) peak to peak. Tests were repeated at different oxidant-fuel ratios to obtain stability limit curves.

The various combustor configurations used in this investigation to deliniate the effects of injection element radial distribution and chamber geometry are shown in table I.

RESULTS AND DISCUSSION

The experiments were performed in both 20 000- and 50 000-pound- (89- and 222-kN-) thrust engines using concentric tube injectors operating at a chamber pressure of 300 psia (2068 kN/m^2 abs (nominal)). The stability characteristics of each configuration were evaluated by ramping the hydrogen injection temperature downward until combustion became unstable. The results and accompanying discussions are presented in the following order:

(1) Effect of element spacing and chamber diameter on stability

(2) Effect of element radial distribution at a constant chamber diameter on stability
(3) Effect of element radial distribution at a constant element spacing on stability
(4) Effect of element radial distribution at other levels of thrust per element on stability
(5) Effect of varying chamber axial flow area on stability
(6) Combustion performance
(7) Application of the response factor model

STABILITY CHARACTERISTICS

Effect of Element Spacing and Chamber Diameter

The experiments to determine the effect of element spacing on acoustic mode instability were conducted using five different 397-element injectors which are shown in figures 3(a) to (e). The thrust chamber diameter was decreased simultaneously with the element spacing and the propellant distribution was uniform across the combustor. (The combustor configurations used in this series are identified as A, B, C, D, and E in table I.) The chamber diameter was varied from 15.70 to 8.35 inches (39.88 to 21.21 cm). The nozzle throat diameter was held constant at 7.82 inches (19.86 cm), necessarily; therefore, contraction ratio varied in this series. The decision to conduct the experiments at a constant nozzle throat diameter and thus, a constant weight flow per element, was made on the basis of reference 2. The results of the referenced investigation showed that variations in total propellant flow per element had a marked effect on stability limits and would mask the effect of element spacing if flow rate were allowed to vary.

The stability characteristics of the five combustor configurations are shown in figure 6. The minimum hydrogen injection temperature for stable combustion for each configuration is presented at an oxidant-fuel ratio of 5. The graph was obtained by cross plotting the hydrogen temperature transition data obtained from tests (such as the one depicted in fig. 5) at several oxidant-fuel ratios. The transition temperature for the 15.70-inch- (39.88-cm-) diameter combustor (configuration E) was not determined because of facility limitations at the time of the test. These results show that stability for uniform propellant distribution is independent of chamber diameter within the range investigated. Screech was encountered at hydrogen injection temperatures between 65° and 70° R (36 and 39 K) for four of the combustor configurations.

In all tests, the mode of instability was identified as the first tangential from amplitude spectral density data. A typical amplitude spectral density plot is shown in figure 7. For the example shown, the maximum pressure amplitude occurred at a fre-

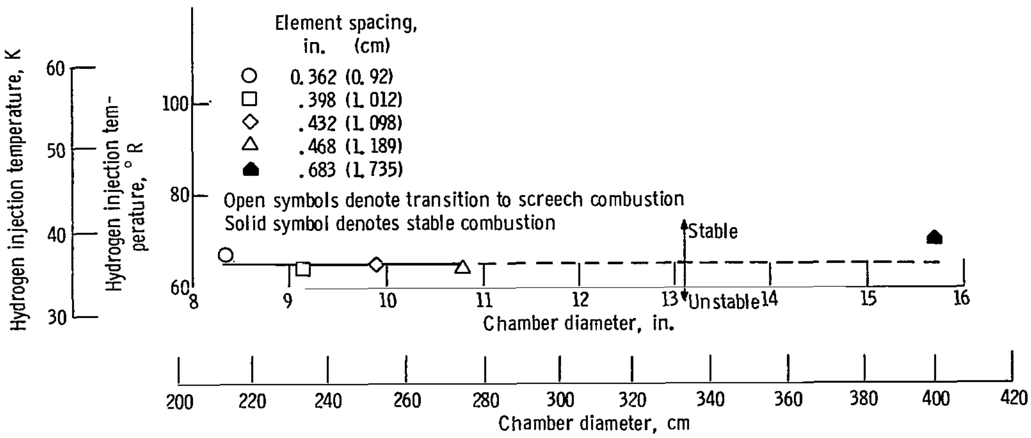

Figure 6. - Effect of varying element spacing and chamber diameter on stability. Injector, 397 elements; nozzle diameter, 7.82 inches (19.86 cm); oxidant-fuel ratio, 5.

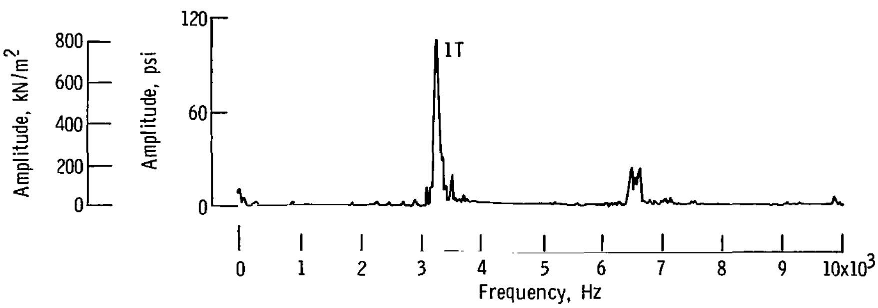

Figure 7. - Typical amplitude spectral density graph for basic combustor. Amplitude, peak to peak; injector, 397 elements; chamber diameter, 10.78 inches (27.38 cm); contraction ratio, 1.9.

quency of about 3200 hertz, which closely corresponds to the calculated frequency for the first tangential acoustic mode for the 10.78-inch- (27.38-cm-) diameter chamber and operating condition.

Effect of Element Radial Distribution at a Constant Chamber Diameter

The same injector configurations were used as in the previous experiments; however, in this series, the chamber diameter and contraction ratio were constant at 10.78 inches (27.38 cm) and 1.9, respectively. The percentage of the 10.78-inch- (27.38-cm-) diameter injector face area covered by a central pattern of active, uniformly distributed injection elements for the four configurations was 100, 85, 72, and 60 percent. (The combustor configurations used in this series are identified as A, F, G, and H in table I.)

The annulus (void of elements) surrounding the injection elements was 0.42, 0.82, and 1.21 inches (1.07, 2.08, and 3.07 cm) wide for the injector configurations with element radial distributions of 85, 72, and 60 percent (of the faceplate area), respectively.

The stability limits in terms of the minimum stable operating hydrogen temperature for the four 10.78-inch- (27.38-cm-) diameter combustor configurations are shown as a function of oxidant-fuel ratio in figure 8. Examination of the results shows a marked

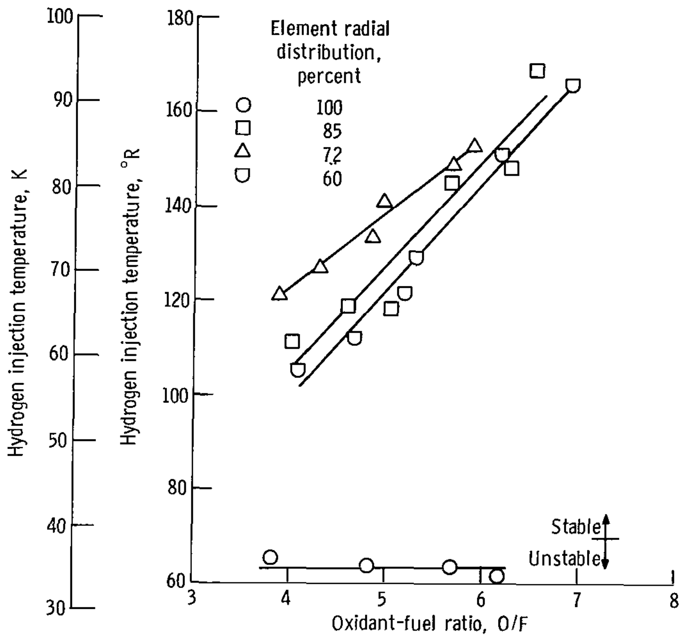

Figure 8. - Effect of varying element radial distribution on stability. Injector, 397 elements; chamber diameter, 10.78 inches (27.38 cm); contraction ratio, 1.9.

effect of varying element radial distribution on stability. At an oxidant-fuel ratio of 5 (fig. 9), the screech transition temperature increased from 64° R (35.5 K) for the 100 percent distribution injector to 128° R (71.1 K) for the 85 percent distribution and to 138° R (77.2 K) for the 72 percent distribution injector. This trend in stability reversed with further reductions in percent distribution. The 60 percent distribution injector had a screech transition temperature of 123° R (68.3 K).

In all tests except those using the 60 percent distribution, 8.35-inch- (21.21-cm-) diameter injector, the mode of instability was first tangential. The predominant mode of instability with the 60 percent distribution injector was first radial with a frequency of about 6500 hertz. With the exception of the change in preferential mode with the 60 percent distribution injector, the trends in stability of the present experiment are not in agreement with previous experimental results. Based on classical acoustic theory (ref. 3) and the results of references 4 and 5, one would expect that removal of energy sources or propellant flow near the walls (antinode of the tangential mode) would reduce the available energy for driving tangential mode oscillations. The changes in propellant

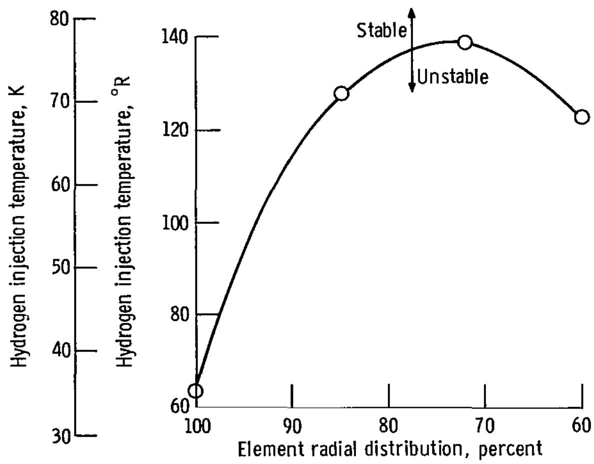

Figure 9. - Effect of varying element radial distribution on stability. Injector, 397 elements; chamber diameter, 10.78 inches (27.38 cm); contraction ratio, 1.9; oxidant-fuel ratio, 5.

response corresponding to changes in element distribution may explain the observed trends as will be discussed in the section APPLICATION OF RESPONSE FACTOR MODEL.

Effect of Element Radial Distribution at a Constant Element Spacing

The effect of varying element radial distribution by changing the thrust chamber diameter on stability is shown in figure 10. Included in the figure are the stability limits of combustor configurations A to M (table I) at an oxidant-fuel ratio of 5. At all chamber diameters, the results show that for maximum stability, the injectors should be designed for uniform distribution without voids at the chamber wall. The combustor configuration that was unstable in the radial mode (configuration H of table I) had a transition temperature inconsistent with the tangential mode limits, as expected.

The results of an attempt to correlate the effect on stability of void areas at the periphery of the combustor are shown in figure 11. In addition to the element distribution parameter used in the figure, parameters consisting of the diameter of outer row of elements divided by the chamber diameter, element spacing (distance between concentric element circles) divided by the chamber diameter and annulus width divided by chamber diameter were examined. The data were not completely correlated by any of the parameters selected. These results indicate that engine stability can be significantly affected by element radial distribution and the trend of decreasing stability with decreasing radial

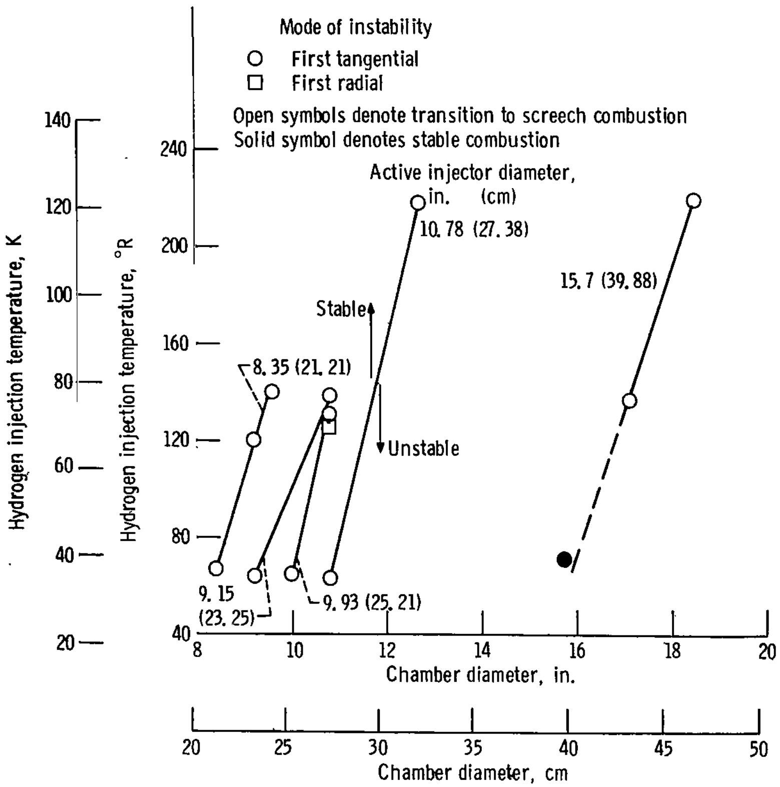

Figure 10. - Effect of varying element radial distribution at constant element spacing on stability. Injector, 397 elements; nozzle throat diameter, 7.82 inches (19.86 cm); oxidant-fuel ratio, 5.

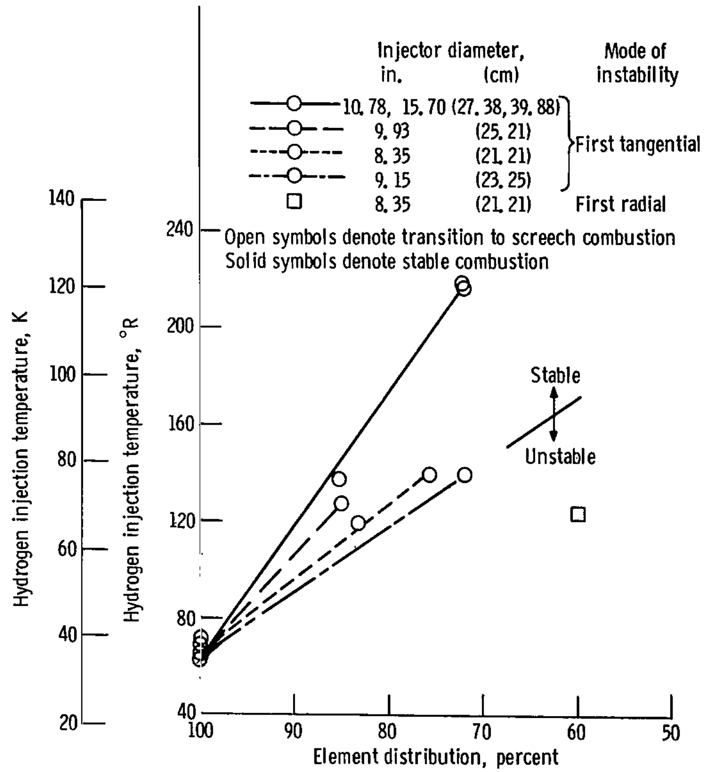

Figure 11. - Effect of varying element radial distribution on stability. Injector, 397 elements; oxidant-fuel ratio, 5.

distribution and spacing appears to be independent of chamber diameter. These effects are not predicted by the stability parameter W_{cr} of reference 2.

Effect of Element Radial Distribution at Other Levels of Thrust Per Element

The results of other experiments to determine if the previous results are applicable to injectors with differing numbers of injection elements are presented in figures 12 to 14. The effect of plugging the outer row of injection elements of a 201-element injector which was marginally stable at 63° R (35 K) is shown in figure 12. The resulting injector configuration had 157 injection elements distributed over 72 percent of the faceplate area (combustor configuration R). According to reference 2, reducing the number of injection elements (higher weight flow per element) should have stabilized the configuration. However, as seen in figure 12, the screech transition temperature at an oxidant-fuel ratio of 5 increased from 63° to 108° R (35 to 60 K) (decreasing combustion stability) which is consistent with the results of figure 11.

Figure 13 shows the effect of decreasing the void annulus width on stability characteristics of a 421-element concentric tube injector which was used in the studies of

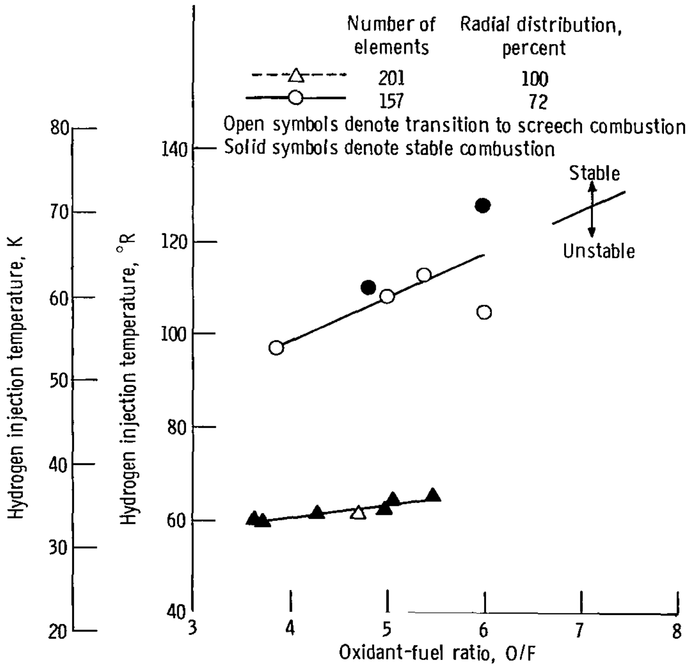

Figure 12. - Effect of varying element radial distribution on stability. Injectors, 157 and 201 elements; chamber diameter, 10.78 inches (27.38 cm); contraction ratio, 1.9.

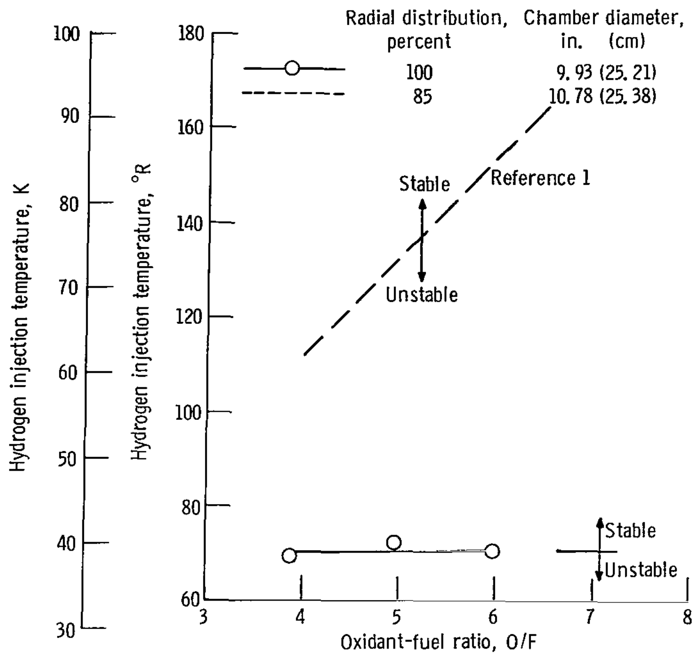

Figure 13. - Effect of reducing annulus width at periphery of injector on stability. Injector, 421 elements; nozzle throat diameter, 7.82 inches (19.86 cm).

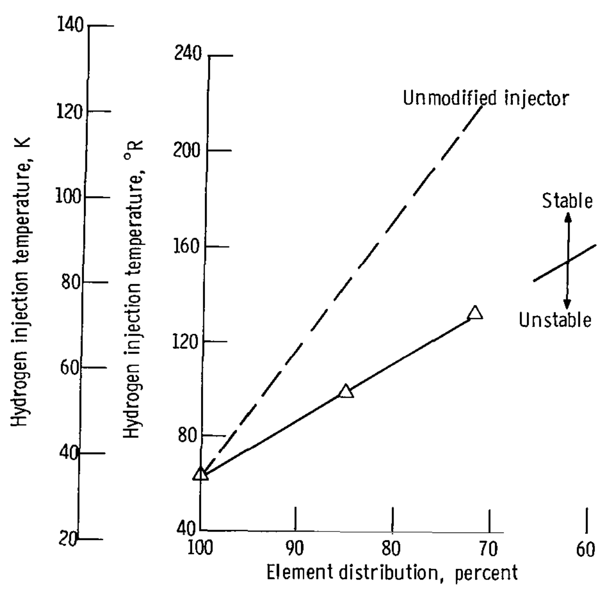

Figure 14. - Effect of varying thrust chamber diameter on stability. Injector, 397 elements; injector diameter, 15.7 inches (39.88 cm); nozzle throat diameter, 12.32 inches (31.3 cm); oxidant-fuel ratio, 5.

references 1 and 2. The thrust chamber diameter was reduced from 10.78 to 9.93 inches (27.38 to 25.21 cm) thereby providing a combustor with uniform or 100 percent distribution (combustor configuration S). The result of this chamber modification was to reduce the screech transition temperature from 130° to about 70° R (72.2 to 38.9 K) (increasing combustion stability). In summary, the destabilizing effect of concentrating the element at the center of the injector and leaving an annulus, void of injection elements, at the periphery of the combustor appears to be independent of the number of injection elements.

The effect of varying thrust chamber diameter from 15.7 to 18.5 inches (39.88 to 47 cm) on stability at a higher thrust level (nozzle throat diameter of 12.32 in. or 31.3 cm) of 50 000 pounds (222 kN) is shown in figure 14. It should be noted that, in addition to the change in nozzle throat diameter, the injection areas were resized (as discussed in the APPARATUS section and noted as configurations N, O, and P in table I) for the higher flow rates corresponding to the 50 000-pound- (222-kN-) thrust operating condition. The hydrogen temperature stable operating limits again varied linearly with element distribution.

Another interesting result of this test series is the general improvement in the stability of the modified injector. This trend is consistent with the predictions of reference 2 that the increased stability results from the increase in oxygen injection orifice diameter.

Effect of Varying Chamber Axial Flow Area

The objective of this test series was to determine the axial length (from the injector) at which chamber diameter could be increased without any effect on stability. The injector with 397 uniformly distributed injection elements in a diameter of 8.35 inches (21.21 cm) was used in this test series. Cylindrical and tapered sleeves or rings were fabricated and installed into a 10.78-inch- (27.38-cm-) diameter chamber as shown in figure 15. The internal diameter of the sleeves was 8.35 inches (21.21 cm). The cylindrical sleeve lengths evaluated included 4, 2, $1\frac{1}{2}$, and 1 inches (10.16, 5.08, 3.81, and 2.54 cm). The tapered sleeve was 2 inches (5.08 cm) long. (The combustor configurations are identified as T, U, V, W, and X in table I.)

The stability results which were cross plotted at an oxidant-fuel ratio of 5 are presented in figure 15. Shown are the screech transition temperatures as a function of sleeve length (measured from the injector face). The combustor incorporating the 4-inch- (10.16-cm-) long cylindrical sleeve had the same stability as the full-length 8.35-inch- (21.21-cm-) diameter combustor. At step variations in chamber diameter at lengths less than 4 inches (10.16 cm), stability continuously decreased to the trans-

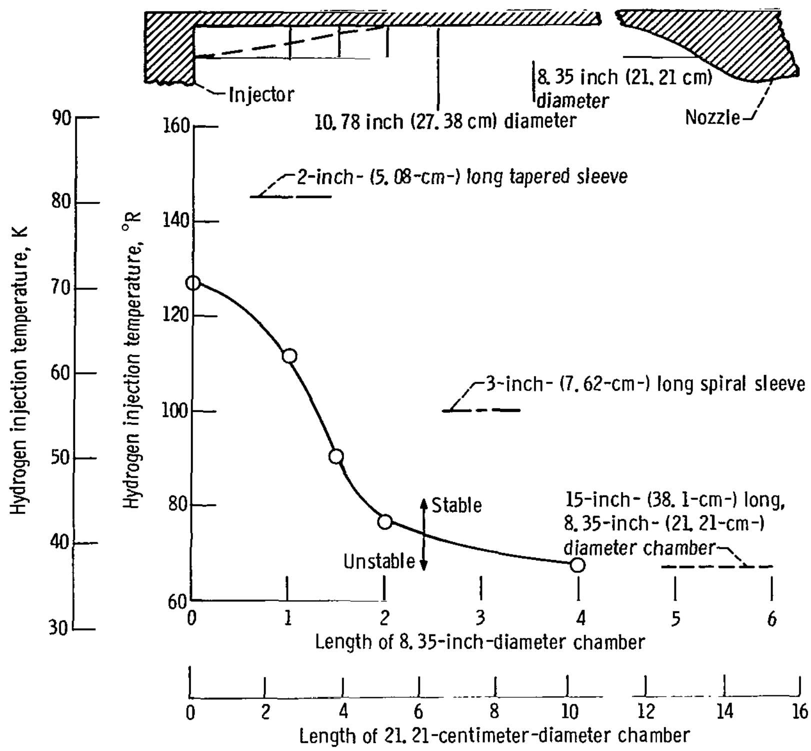

Figure 15. - Effect of variable area thrust chamber on stability. Injector, 397 elements; throat diameter, 7.82 inches (19.86 cm); oxidant-fuel ratio, 5.

ition temperature (123° R or 68.3 K) of the injector in a 10.78-inch- (27.38-cm-) diameter combustor. The major effect of changes in diameter on stability occurred within 2 inches (5.08 cm) of the injector. The stability limit with the 2-inch- (5.08-cm-) long tapered sleeve (indicated by the dashed line in fig. 15) was 20° R (11.1 K) above the 10.78-inch- (27.38-cm-) diameter baseline configuration. This anomaly is unexplained.

In addition to the cylindrical and tapered sleeve experiments, a few tests were conducted with a 3-inch- (7.62-cm-) long, spiral sleeve shown in table I and identified as configuration Y. The internal radius of the sleeve varied from 4.18 to 5.39 inches (10.62 to 13.69 cm). It was hypothesized that the radial step of the sleeve would interfere with spinning tangential waves and thus improve the stability characteristics of the combustor. An improvement in stability resulted as compared to the "no sleeve" case, but complete stabilization was not achieved. At an oxidant-fuel ratio of 5, transition into instability occurred at a hydrogen temperature of about 100° R (55.6 K) or 30° R (16.7 K) above that of a 3-inch (7.62-cm-) long cylindrical sleeve (fig. 15).

In a 10.78-inch- (27.38-cm-) diameter thrust chamber, combustion was determined to be complete by pitot tube measurements at an axial length between 3 and 4 inches (7.62 and 10.16 cm) for the injection element used. Thus, it appears that the critical length of 4 inches (10.16 cm), beyond which changes in flow area have no effect on stability, is associated with the length of the combustion zone.

COMBUSTION PERFORMANCE

Characteristic exhaust velocity efficiency at the minimum stable operating hydrogen injection temperature is presented for each test conducted in the program in table II. It should be noted that these data were obtained under transient conditions; thus, a considerable amount of scatter due to instrument time constant variations and hydrogen propellant mass accumulation in the propellant line, manifold, and injector cavity is present in the results. Some typical performance data at hydrogen injection temperatures varying between 120° and 160° R (66.7 and 188.9 K) are shown in figure 16. These results were obtained prior to the initiation of the hydrogen temperature ramp, thus, without the error of mass accumulation. In general, the combustion performance of the 397-element concentric tube injector was about $98\frac{1}{2}$ percent of theoretical shifting characteristic exhaust velocity. Variations in element spacing and chamber diameter had no apparent effect on performance. The performance data were corrected for momentum pressure loss, but not for heat transfer to the combustor walls.

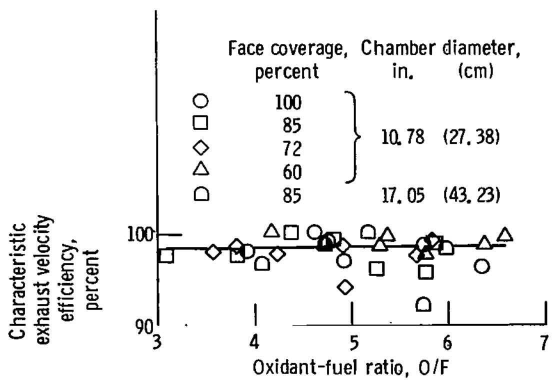

Figure 16. - Combustion performance of 397-element concentric tube injectors at hydrogen injection temperatures between 120° to 160° R (66.7 to 88.9 K). Contraction ratio, 1.9.

APPLICATION OF RESPONSE FACTOR MODEL

In reference 2, a special form of the response factor model was found to predict combustor stability limits as determined by hydrogen injection temperature (density) for changes in chamber pressure, flow per element, and contraction ratio. The investigation discussed herein involves changes of radial injection distribution which were not considered in that form of the model described in reference 2. Therefore, a more general form of the response factor model was derived to include variations of transverse injection distribution and oxygen response.

The response factor model considers the balance of system losses and gains at the stability boundary. The system was assumed to be characterized by (1) the hydrogen gas flow through the injector, (2) the liquid oxygen atomization, and (3) the combustion gas flow in the chamber and through the nozzle. The influence of each loss and gain was expressed in the form of a response quantity that was weighted according to the respective mass flow. That is, for negligible chamber wall losses, the stability limit is given by

$$\dot{w}_T N_T = \dot{w}_H N_H + \dot{w}_{ox} N_{ox} \tag{1}$$

where the N's are complex quantities denoting the ratio of mass flow perturbation to pressure perturbation. The symbols are defined in the appendix. Reference 2 used the special case where (1) nozzle response, (2) oxygen response at a value obtained for a vaporization-limited process, (3) oscillation frequency, and (4) combustion efficiency were all constant. The more general form assumed for this study to account for injection element distribution effects provided for (1) nozzle response as a function of oscillation frequency and geometry, (2) chamber geometry, (3) hydrogen response as a function of oscillation frequency, and (4) oxygen response as a function of oscillation frequency and mean jet breakup time for an atomization-limited process. Efficiency was again assumed constant to provide values for the operating conditions.

Initial calculations indicated that the vaporization-limited response of the oxygen was too low (real component no larger than 0.55) to provide a balance of the type given by equation (1). However, the atomization-limited oxygen response was large enough to match the other responses. Therefore, the oxygen response was assumed to be sufficiently represented by the atomization-limited process.

The model is used to examine the operating conditions during a transition from stable to unstable operation. If acoustic flow oscillations are to occur during this transition, it is assumed as in reference 6 that the flow oscillations must match the flow response at the nozzle end of the chamber and the flow response at the injector end of the chamber. The flow response at the nozzle is given by

$$\left(\frac{w'}{p'}\right)_N = \frac{1}{\gamma}\left(1 + \frac{\gamma}{M}\frac{v'}{p'}\right) = G \tag{2}$$

where $\gamma\, v'/p'$ is the irrotational admittance coefficient from page 53 of reference 7. This is in turn used to calculate the quantity

$$C = -\left[\frac{B_1(1 - M^2 + \gamma G M^2) + \omega(\gamma G - 1)M}{B_2(1 - M^2 + \gamma G M^2) + \omega(\gamma G - 1)M}\right] \tag{3}$$

from which N_T is obtained from the following equation:

$$N_T = \frac{1}{\gamma}\left\{1 - \frac{B_1 e^{-iLB_1} + B_2 C e^{-iLB_2}}{M\left[\omega\left(e^{-iLB_1} + C e^{-iLB_2}\right) + M\left(B_1 e^{-iLB_1} + B_2 C e^{-iLB_2}\right)\right]}\right\} \tag{4}$$

where

$$B_1 = \frac{\omega M + \sqrt{\omega^2 M^2 + (M^2 - 1)(m^2 - \omega^2)}}{1 - M^2}$$

and

$$B_2 = \frac{\omega M - \sqrt{\omega^2 M^2 + (M^2 - 1)(m^2 - \omega^2)}}{1 - M^2}$$

The response obtained from these equations can be used when the flow properties are uniform in the transverse direction. To correct N_T for variations of transverse injection distribution, a correction factor was obtained from reference 4. Reference 4 describes the acoustic gains in terms of an interaction index n and a sensitive time lag

T_n such that

$$A_{\nu\eta}\left[n\left(1 - e^{-i\omega T_n}\right)\right] = N_T \tag{5}$$

for a process that is only pressure sensitive. The pressure distribution coefficient $A_{\nu\eta}$ is defined in equation (19a) of reference 4. As the propellant injection is changed from a uniform distribution to injection concentrated near the centerline of the chamber, $A_{\nu\eta}$ decreases for the first tangential acoustic mode. With the aid of equation (11) in reference 8, equation (5) becomes

$$A_{\nu\eta}\left(\frac{\dot{w}_H N_H + \dot{w}_{ox} N_{ox}}{\dot{w}_T}\right) = N_T \tag{6}$$

The theoretical studies that have been made to date (e.g., ref. 6) show a strong dependence of the stability on Mach number. In the present investigation, the Mach number was varied from 0.10 to 0.66. Reference 6 is the only study that considers Mach numbers higher than 0.30 and so it was chosen to be used in the present formulation. However, reference 6 is limited in application to a pressure-sensitive process. Therefore, the velocity-sensitive effects were excluded in this analysis.

Details of the hydrogen response analysis are given in reference 9. The results are given in terms of the maximum ratio of flow rate perturbation w' to pressure perturbation p' (eq. (24) of ref. 9) and the phase angle θ between w' and p' (eq. (25) of ref. 9). The real component of the hydrogen response is the part of w' that is in phase with p' and is given in reference 8 as

$$R_1 = \frac{2}{T(p'_{max})^2}\int_0^T w'(t)p'(t)dt \tag{7}$$

The imaginary component is the part of w' that is in quadrature with p' and is given in reference 8 as

$$I_1 = \frac{2}{T(p'_{max})^2}\int_0^T w'(t)p'\left(t + \frac{T}{4}\right)dt \tag{8}$$

For $T = 2\pi$, then, the hydrogen response is

$$N_H = R_1 + iI_1 = \left(\frac{w'}{p'}\right)_{max} (\cos\theta + i\sin\theta) \tag{9}$$

where $(w'/p')_{max}$ and θ are given by equations (24) and (25) in reference 9.

The response of the oxygen was calculated for the jet atomization model of reference 10 as

$$N_{ox} = \frac{\sin(0.15\,\omega\tau)}{0.15\,\omega\tau\gamma}\left[\frac{\sin\omega\tau}{\omega\tau} - \cos\omega\tau + i\left(\frac{1-\cos\omega\tau}{\omega\tau} - \sin\omega\tau\right)\right] \tag{10}$$

The response of the jet atomization process was shown in reference 10 to be a significant gain in stability considerations and a function of oscillation frequency and mean jet breakup time τ. In order to provide a prediction of stability, the oscillation frequency and jet breakup time must be given.

An attempt was made to measure the experimental oscillation frequency at the onset of instability to provide values as input to the model. Changes in oscillation frequency of 0.5 percent can radically change the model predictions. The measured frequencies were within ±5 percent of the acoustic (closed-end chamber) frequency; thus, the experimental error of frequency measurement was too large to provide meaningful values. The values of oscillation frequency that were subsequently determined (theoretically) were within ±10 percent of the acoustic (closed-end chamber) frequency.

A determination of the jet breakup time was equally formidable. The jet breakup time was determined experimentally in reference 11 to be given by

$$\tau = \frac{D_{ox}}{V_R}\sqrt{\frac{\rho_{ox}}{\rho_g}\epsilon} \tag{11}$$

where V_R and ρ_g are the relative velocity and density of the gas surrounding the liquid jet and ϵ is a constant to characterize the extent of liquid jet breakup. There was obvious difficulty in describing the gas surrounding the liquid oxygen jet in the engine. Therefore, the jet breakup time was considered unknown.

A review of the equations shows that a prediction of stability can be made only if the oscillation frequency and the jet breakup time are known. Since the experimental oscillation frequency and jet breakup time are essentially indeterminable, the oxygen response (eq. (6)) could not be determined. Therefore, the following approach was used to solve for the oxygen response: The experimental stability limit in terms of hydrogen injection temperature was used to calculate the hydrogen response N_H. The response N_T was calculated for a range of oscillation frequencies using equation (4). With the pressure distribution coefficient calculated and the propellant injection flow rates known, equation (6) was used to determine the oxygen response N_{ox} for various oscillation frequencies. This result combined with equation (10) was used to finally determine the jet breakup time τ.

The jet breakup times that were needed to satisfy the experimental results were correlated by a parameter that is easily identified with equation (11) and shown in figure 17. The jet breakup time τ obtained from the correlating parameter is

$$\tau = 9.05 \frac{D_{ox}}{V_T V_H^{1.25}} \sqrt{\frac{PA_H^2}{\rho_T \rho_H^{0.25} (\Delta d)^3}} \tag{12}$$

where Δd was the spacing of the concentric circles of injection elements used in the design of the injectors for this study. Included are the data from references 1 and 2. The scatter of the points from the values of jet breakup time determined from equation (12) is much too large to allow predictions of stability limits. However, a comparison of equations (11) and (12) can indicate the plausibility of the response factor model chosen.

The parameter within the square root of equation (12) may be related directly to the surrounding gas density and the $V_T V_H^{1.25}$ may be related directly to the relative gas velocity. Intuitively, the gas surrounding the liquid oxygen jet would seem to be made up of the combustion gas and the hydrogen gas. Independent variation of any one of these parameters seems to be consistent with equation (11).

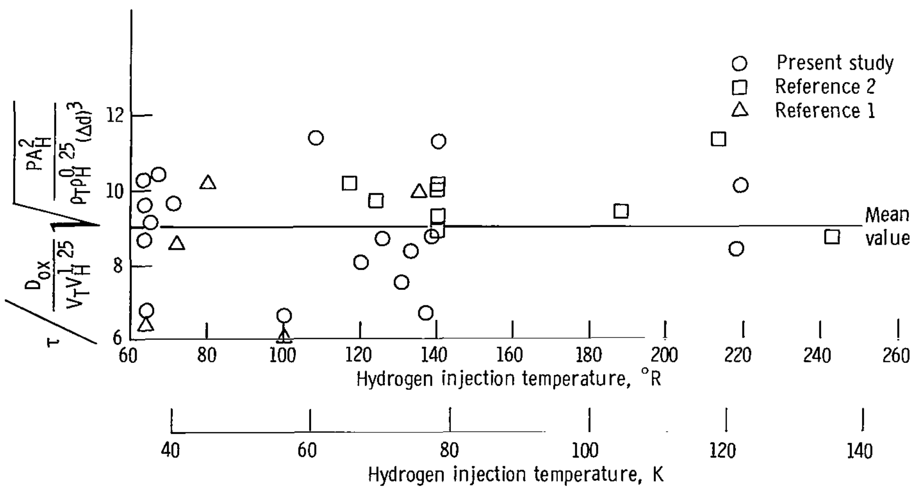

Figure 17. - Correlating parameter used to indicate effects of operating conditions on jet breakup time determined from response factor model.

This analysis illustrates that changes in element distribution for the injection of propellants can affect combustion response such that the geometric, acoustic effects described by the pressure distribution coefficient of reference 4 are reversed. Specifically, the jet breakup time determines the oxygen response. Since the breakup time is dependent on the density and velocity of the medium surrounding the jet, any geometric change (and/or change of element distribution) will change the oxygen response. In this study the oxygen response has an effect so strong as to overcome the effects for the case of energy addition at the pressure antinode.

SUMMARY OF RESULTS

The effect of varying element radial injection distribution and chamber geometry on acoustic mode instability was investigated using 20 000- and 50 000-pound (89- and 222-kN-) thrust size engines. The tests were conducted at a chamber pressure of 300 psia (2070 kN/m^2 abs) and over a range of oxidant-fuel ratios from 4 to 6.5. This investigation yielded the following results:

1. Providing an annulus, void of injection elements, at the perimeter of the injector reduced tangential-mode stability.

2. The destabilizing effect of the annulus at the perimeter of the injector appeared to be independent of the number of injection elements (thrust per element) and chamber diameter.

3. Inserting a partial-length sleeve 4 inches (10.16 cm) long into the annulus at the perimeter of the injector provided the same stability as a full-length chamber sleeve. The length of sleeve required to produce the same stability as the full-length chamber could be related to the length of the combustion zone.

4. A 3-inch- (7.62-cm-) long spiral sleeve inserted into the annulus at the injector perimeter increased stability of the combustor but was not as effective as the 3-inch- (7.62-cm-) long cylindrical sleeve.

5. Combustion performance was not affected by variations in element spacing over the range investigated.

6. A response factor model which included a transverse injection distribution correction and a variable oxygen response for an atomization controlled process was used to obtain a correlation equation for the oxygen jet breakup time. The correlation equation agrees qualitatively with an empirical equation obtained previously in steady-state experiments.

7. The correlation equation developed in the present study for oxygen jet breakup time cannot be used quantitatively for predictions of stability.

8. In this study the oxygen response (atomization controlled) was large enough to outweigh the effects expected from a strict consideration of energy addition as related to radial injection distribution.

Lewis Research Center,
National Aeronautics and Space Administration,
Cleveland, Ohio, May 5, 1969,
128-31-51-03-22.

APPENDIX - SYMBOLS

$\mathcal{A}$ nozzle contraction ratio

A_H total injection area of hydrogen, ft^2 (m^2)

$A_{\nu\eta}$ pressure distribution coefficient where ν is tangential mode number and η is radial mode number

C defined by eq. (3)

D_{ox} oxygen injection diameter, in. (cm)

Δd element circle-to-circle spacing, in. (cm)

e exponential

G defined by eq. (2)

I_1 imaginary component of hydrogen response

i $\sqrt{-1}$

L length of combustion chamber/radius of combustion chamber, dimensionless

M Mach number of combustion gas as it enters nozzle

m mode number (1.8413 for first tangential mode, 3.0543 for second tangential mode, and 3.8317 for first radial mode)

N complex response factor, dimensionless

n pressure interaction index, dimensionless

P combustion chamber total pressure, psia (kN/m^2 abs)

p' pressure perturbation, dimensionless

R_1 real component of hydrogen response, dimensionless

T period of oscillation, rad

T_n sensitive time lag, dimensionless

t time, sec

V flow velocity, ft/sec (m/sec)

v' axial velocity perturbation, dimensionless

$\dot{w}$ flow rate, lbm/sec (kg/sec)

w' flow rate perturbation, dimensionless

γ specific heat ratio

ϵ critical distortion factor, dimensionless

θ phase angle between hydrogen w' and p'

ρ density, lbm/ft^3 (kg/m^3)

τ jet breakup time, sec

ω frequency of oscillation, rad/sec

Subscripts:

g gas

H hydrogen gas

max maximum value

N exhaust nozzle

ox oxygen liquid

R relative quantity

T final gas products

REFERENCES

1. Wanhainen, John P.; Parish, Harold C.; and Conrad, E. William: Effect of Propellant Injection Velocity on Screech in 20,000-Pound Hydrogen-Oxygen Rocket Engine. NASA TN D-3373, 1966.

2. Wanhainen, John P.; Feiler, Charles E.; and Morgan, C. Joe: Effect of Chamber Pressure, Flow Per Element, and Contraction Ratio on Acoustic-Mode Instability in Hydrogen-Oxygen Rockets. NASA TN D-4733, 1968.

3. Rayleigh, John W. S.: The Theory of Sound. Vol. 2. Dover Publications, 1945, p. 226.

4. Reardon, F. H.; McBride, J. M.; and Smith, A. J., Jr.: Effect of Injection Distribution on Combustion Stability. AIAA J., vol. 4, no. 3, Mar. 1966, pp. 506-512.

5. Zucrow, M. J.; Osborn, J. R.; and Bonnell, J. M.: High Frequency Combustion Pressure Oscillations in Motors Burning Gaseous Propellants. Rep. JPC-409, TM-65-5, Purdue University, Aug. 1965. (Available from DDC as AD-478023.)

6. Priem, Richard J.; and Rice, Edward J.: Combustion Instability with Finite Mach Number Flow and Acoustic Liners. Presented at the Twelfth Symposium (International), on Combustion, Poitiers, France, July 14-20, 1968.

7. Crocco, Luigi; and Sirignano, William A.: Behavior of Supercritical Nozzles under Three-Dimensional Oscillatory Conditions. AGARD ograph-117, 1967.

8. Crocco, L.: The Relevance of a Characteristic Time in Combustion Instability. Second ICRPG Combustion Conference. Rep. CPIA Publ. No. 105, Vol. 1, Applied Physics Lab., Johns Hopkins Univ., May 1966, pp. 115-138.

9. Feiler, Charles E.; and Heidmann, Marcus F.: Dynamic Response of Gaseous-Hydrogen Flow System and its Application to High-Frequency Combustion Instability. NASA TN D-4040, 1967.

10. Heidmann, M. F.; and Groeneweg, J. F.: Dynamic Behavior of Liquid Jet Atomization. Fifth ICRPG Combustion Conference. Rep. CPIA Publ. No. 183, Applied Physics Lab., Johns Hopkins Univ., Dec. 1968, pp. 111-117.

11. Clark, Bruce J.: Breakup of a Liquid Jet in a Transverse Flow of Gas. NASA TN D-2424, 1964.

TABLE I. - COMBUSTOR CONFIGURATIONS

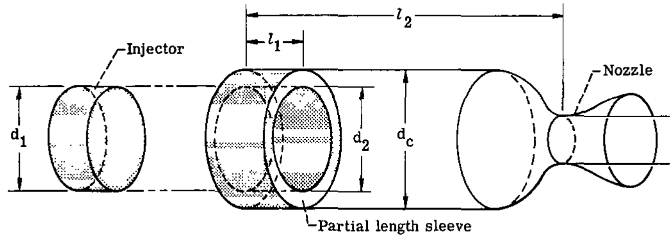

Configurations A to X

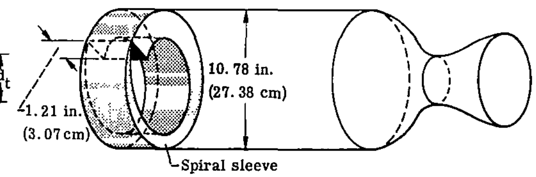

Configuration Y

Config-uration	Number of elements	Active injector diameter, d_1		Internal sleeve diameter, d_2		Internal chamber diameter, d_c		Throat diameter, d_t		Contraction ratio	Sleeve length, l_1		Chamber length, l_2		Injection areas				Element spacing		Element distri-bution, percent	Test objective
															Hydrogen		Oxygen					
		in.	cm	in.	cm	in.	cm	in.	cm		in.	cm	in.	cm	sq in.	sq cm	sq in.	sq cm	in.	cm		
A	397	10.78	27.38	10.78	27.38	10.78	27.38	7.82	19.86	1.9	0	0	18.5	47	4.36	28.11	0.839	5.41	0.468	1.189	100	Effect of element spacing and chamber diameter; effect of element radial distribution for various element spacings
B	↓	9.93	25.21	9.93	25.21	9.93	25.21	↓	↓	1.61	↓	↓	18	45.7	↓	↓	↓	↓	.432	1.098	↓	
C		9.15	23.25	9.15	23.25	9.15	23.25			1.37			↓	↓					.398	1.012		
D		8.35	21.21	8.35	21.21	8.35	21.21			1.14									.362	.92		
E		15.7	39.88	15.7	39.88	15.7	39.88			4.02			19.5	49.5					.683	1.735		
F	397	9.93	25.21	9.93	25.21	9.93	25.21	7.82	19.86	1.9	0	0	18	45.7	4.36	28.11	0.839	5.41	.432	1.098	85	Effect of element radial distribution at constant chamber diameter; effect of element radial distribution for various element spacings
G	↓	9.15	23.25	9.15	23.25	9.15	23.25	↓	↓	↓	↓	↓	↓	↓	↓	↓	↓	↓	.398	1.012	72	
H		8.35	21.21	8.35	21.21	8.35	21.21												.362	.92	60	
I	397	8.35	21.21	9.61	24.41	9.61	24.41	7.82	19.86	1.51	0	0	18	45.7	4.36	28.11	0.839	5.41	0.362	0.92	75	Effect of element radial distribution for various element spacings
J	↓	8.35	21.21	9.15	23.25	9.15	23.25	↓	↓	1.37	↓	↓	↓	↓	↓	↓	↓	↓	.362	.92	83	
K		10.78	27.38	12.72	32.31	12.72	32.31			2.61									.468	1.189	72	
L		15.7	39.88	17.05	43.31	17.05	43.31			4.75			19.5	49.5					.683	1.735	85	
M		15.7	39.88	18.5	47.0	18.5	47.0			5.6			19.5	49.5					.683	.735	72	
N	397	15.7	39.88	15.7	39.88	15.7	39.88	12.32	31.3	1.61	0	0	30	76.2	8.10	52.25	2.045	13.2	0.683	1.735	100	
O	↓	↓	↓	17.05	43.31	17.05	43.31	↓	↓	1.9	↓	↓	↓	↓	↓	↓	↓	↓	↓	↓	85	Effect of element radial distribution at other levels of thrust per element
P				18.5	47.0	18.5	47.0			2.23											72	
Q	201	10.78	27.38	10.78	27.38	10.78	27.38	7.82	19.86	1.9			18.5	47	3.69	23.81	.607	3.92	.609	1.546	100	
R	157	9.15	23.25	10.78	27.38	10.78	27.38	↓	↓	1.9			18.5	47	2.88	18.58	.474	3.06	.609	1.546	72	
S	421	9.93	25.21	9.93	25.21	9.93	25.21			1.61	↓	↓	18	45.7	4.62	29.8	.89	5.74	.455	1.155	100	
T	397	8.35	21.21	8.35	21.21	8.35	21.21	7.82	19.86	1.9	4	10.16	18	45.7	4.36	28.11	0.839	5.41	0.362	0.92	---	
U											2	5.08									---	Effect of variable area thrust chamber geometry
V											1.5	3.81									---	
W				↓	↓						1	2.54									---	
X				Tapered	-----						2	5.08	↓	↓							---	
Y	↓	↓	↓	Spiral	-----	↓	↓	↓	↓	↓	3	7.62	18.5	47	↓	↓	↓	↓	↓	↓	---	

TABLE II. - EXPERIMENTAL DATA

(a) U.S. customary units

Combustor configuration	Test	Chamber diameter, in.	Number of injection elements	Element radial distribution, percent	Contraction ratio, $\mathscr{A}$	Hydrogen injection temperature, ^{o}R	Chamber pressure at injector face, psia	Oxidant-fuel ratio, O/F	Efficiency of characteristic exhaust velocity, percent	Propellant weight flow, lb/sec		Injection velocity, ft/sec		Injector pressure drop, psi		Stability classification
										Hydrogen	Oxygen	Hydrogen	Oxygen	Hydrogen	Oxygen	
A	292	10.78	397	100	1.9	114.0	317	4.85	102.0	10.09	48.92	630	111.0	47.9	134	Stable
	---					-----	---	----	-----	-----	-----	---	-----	-----	---	---------
	294					63.3	346	4.84	97.3	11.56	55.90	139	127	11.5	181	Transition
	295					65.4	326	3.83	93.1	13.42	51.45	188	117.0	20.01	157	
	296					63.3	338	5.67	96.1	10.28	58.29	124	133.0	9.81	192	
	297					61.9	335	6.19	93.5	9.90	61.25	113	139.0	10.60	217	
B	772	9.93	397	100	1.61	64.3	314	4.47	98.2	10.93	48.85	135	111	8.86	151	Transition
	773					61.9	313	5.43	100.4	9.35	50.76	502	115	14.4	157	Stable
	---					-----	---	----	-----	-----	-----	-----	-----	-----	---	---------
	775					62.5	312	5.98	100.9	8.71	52.12	98.1	118	6.98	176	Transition
	776					59.6	313	3.61	99.9	12.45	44.99	124	102	14.69	139	Stable
C	552	9.15	397	100	1.37	64.7	307	4.99	89.1	10.39	51.89	145	120	8.51	171	Transition
	553					64.7	304	3.93	90.6	11.96	46.97	168	108	8.71	141	
	554					64.0	311	5.53	90.9	9.65	53.34	126	122	9.76	195	
	555					62.3	319	4.34	90.1	11.74	50.97	137	116	13.73	161	
	556					62.6	318	5.70	92.3	9.55	54.46	114	124	12.03	220	
D	369	8.35	397	100	1.14	65.5	297	3.82	88.0	11.31	43.16	233	129	15.17	113	Transition
	370					71.2	296	4.71	90.64	9.80	46.18	287	101	20.64	122	
	371					58.5	314	5.56	87.70	9.64	53.56	147	117	24.94	200	
	372					58.0	315	4.70	89.21	10.62	49.96	218	107	32.81	157	
	373					57.6	318	3.67	88.7	12.81	47.04	181	101	38.84	155	

E	262	15.70	397	85	4.02	75.9	327	3.55	94.2	12.59	44.73	338	110	13.70	123	Stable
	---					-----	---	----	-----	-----	-----	----	---	-----	---	
	265					69.2	307	4.75	90.2	10.46	49.68	219	115	12.84	143	
	266					73.2	305	3.88	80.7	13.48	52.36	359	121	20.27	166	
	---					-----	---	----	-----	-----	-----	----	---	-----	---	
	---					-----	---	----	-----	-----	-----	----	---	-----	---	
	269					65.0	305	3.93	80.2	13.49	52.96	182	121	19.25	176	
	270					65.0	307	3.97	78.8	13.71	54.41	183	125	13.96	175	
F	358	10.78	397	72	1.9	118	299	5.03	99.4	9.60	48.28	690	110	35.82	151	Transition
	360					105	306	3.24	97.5	13.63	44.19	786	101	53.42	111	Stable
	361					111	299	4.01	97.8	11.30	45.26	738	103	46.63	129	Transition
	362					169	316	6.51	95.9	8.57	55.78	809	128	38.92	200	
	363					145	297	5.66	96.1	8.90	50.39	789	114	38.17	160	
	364					118	296	4.61	100.5	10.27	47.30	713	107	39.44	142	
	365					148	296	6.26	99.0	8.35	52.31	745	119	37.16	171	
G	546	10.78	397	72	1.9	136	319	3.82	109.2	12.25	46.84	911	108	65.2	125	Stable
	547					121	311	3.88	97.2	12.20	47.30	799	110	46.38	144	Transition
	548					141	316	4.95	97.9	10.36	51.25	808	118	48.74	157	
	549					153	317	5.88	97.4	9.32	54.78	794	125	39.48	190	
	550					127	315	4.30	96.3	11.59	49.83	788	114	49.99	148	
	551					147	317	5.66	96.7	9.64	54.58	793	126	-----	---	
H	347	10.78	397	60	1.9	122	296	5.16	92.9	9.94	51.33	731	116	36.73	179	Transition
	348					105	301	4.11	94.1	11.44	46.98	668	106	45.02	142	
	349					181	314	6.82	101.2	8.10	55.25	868	123	38.69	298	
	350					166	310	6.86	100.0	8.06	55.31	567	122	31.14	186	
	351					122	312	4.69	98.7	10.54	49.47	596	111	37.71	160	
	352					151	314	6.16	99.4	8.81	54.23	600	120	34.13	176	
	353					129	303	5.29	98.5	9.62	50.88	664	115	41.07	157	

TABLE II. - Continued. EXPERIMENTAL DATA

(a) Continued. U.S. customary units

Combustor configuration	Test	Chamber diameter, in.	Number of injection elements	Element radial distribution, percent	Contraction ratio, $\mathscr{A}$	Hydrogen injection temperature, ^{o}R	Chamber pressure at injector face, psia	Oxidant-fuel ratio, O/F	Efficiency of characteristic exhaust velocity, percent	Propellant weight flow, lb/sec		Injection velocity, ft/sec		Injector pressure drop, psi		Stability classification
										Hydrogen	Oxygen	Hydrogen	Oxygen	Hydrogen	Oxygen	
I	478	9.61	397	75.5	1.51	136.8	309	5.04	96.2	9.84	50.71	739.8	112.5	34.62	146.6	Transition
	479					127.1	305	3.75	93.9	12.33	46.88	861.6	104.8	63.55	136.8	
	480					166.2	312	6.29	96.4	8.59	54.93	798.1	122.7	39.04	167.9	
	481					129.8	309	4.39	95.3	10.94	48.88	773.1	109.1	55.77	133.4	
	482					156.9	312	5.62	95.9	9.28	53.05	807.6	118.6	36.50	159.9	
	483					146.7	310	4.93	95.0	10.13	50.76	822.4	113.8	42.65	143.3	
J	484	9.16	397	83.5	1.37	119.7	305.1	4.88	93.9	9.94	50.40	644.5	110.2	46.82	135.8	Transition
	485					82.6	307	3.99	92.3	11.70	49.08	422.9	105.9	34.68	151.6	
	486					135.1	310	6.19	97.9	8.32	52.64	615.2	116.8	24.52	157.9	
	487					111.6	302	4.41	93.3	10.64	48.29	636.9	106.4	24.44	146.3	
	488					132.8	310	5.62	97.2	8.92	51.35	645.4	113.7	38.96	139.5	
	489					103.1	307	3.89	94.6	11.64	46.96	613.9	102.9	51.74	116.6	
K	414	12.72	397	72	2.61	218.5	306.9	4.83	96.22	10.45	51.31	1402	114	62.79	161.7	Transition
	416					169.7	310	3.63	98.57	12.83	47.05	1304	106	72.15	120.4	Transition
	417					249.6	313	5.71	94.29	9.67	57.52	1460	125	81.07	-----	Stable
	418					248.2	312	6.01	95.73	9.16	55.69	1378	125	72.36	190.6	Stable
	419					246.0	308	6.03	94.83	9.12	55.37	1377	125	67.94	191.9	Transition
	422					188.9	307	4.82	95.03	10.58	52.25	1219	116	76.31	161.1	Stable
	425					176.2	311	3.79	98.88	12.40	49.12	1311	106	77.01	126.6	Transition
	426					219.8	315	5.77	97.95	9.29	54.69	1224	122	78.39	168.3	Stable
	427					280.2	313	6.19	94.81	9.06	56.66	1261	127	92.29	236.4	Stable
	428					191.9	306	5.15	94.40	10.14	53.27	1191	118	87.72	206.4	Stable

L	240	17.05	397	85	4.75	189.4	315	5.08	100.4	9.97	50.63	1044	117	58.64	148	Stable
	241					142	308	5.05	95.5	10.25	51.75	796	120	39.7	174	Transition
	243					155	314	5.93	101.1	9.15	54.26	772	127	39.1	169	
	244					144	312	4.70	96.4	11.16	52.50	872	122	43.4	156	
	245					121	312	4.11	93.4	12.71	52.27	806	121	51.13	167	
	246					134	311	5.72	88.2	10.64	60.90	765	140	43.22	224	
M	285	18.5	397	72	5.6	265	318	5.28	103.1	10.03	52.93	1474	119	70.9	166	Transition
	286					190	314	4.22	101.9	11.54	48.68	1214	112	80.7	149	
	287					274	303	6.92	101.2	8.39	58.05	1338	126	70.7	190	
	288					241	315	4.84	96.9	10.95	53.04	1484	122	80.2	176	
	295					227	309	5.08	102.9	9.66	49.09	1242	112	76.16	143	Stable
	297					217	310	4.93	100.3	10.16	50.09	1242	115	70.1	151	Transition
	298					190	314	4.02	97.5	12.38	49.74	1302	112	82.7	150	
	299					249	314	5.85	94.2	9.89	57.83	1378	131	83.9	214	
	300					190	312	4.96	92.5	11.19	55.53	1187	124	78.8	178	
N	386	15.70	397	100	1.61	70.4	314	4.33	95.3	27.9	120.0	------	108	14.7	137.5	Transition
	387					75.54	310	4.46	86.25	29.86	129.8	286.8	122	21.20	294.7	
	388					62.0	333	5.19	98.77	25.18	125.74	136.3	119.7	4.56	129.7	
O	375	17.05	397	85	1.9	47.81	310	4.85	97.28	25.70	123.7	629	114	36.63	121.3	Transition
	376					95.35	309	3.94	94.7	30.2	119	------	107	38.68	127.3	
	377					113.3	300	6.21	97.84	21.06	127.3	657	120	36.68	134.9	
	378					79.6	306	4.58	89.1	28.3	127.5	------	116	23.17	146.3	
	379					103.1	300	5.62	98.61	22.28	123.9	611	115	26.86	125.1	
	380					90.2	302	4.67	94.4	29.5	117.9	-----	108	41.50	111.5	

TABLE II. - Continued. EXPERIMENTAL DATA

(a) Concluded. U.S. customary units

Combustor configuration	Test	Chamber diameter, in.	Number of injection elements	Element radial distribution, percent	Contraction ratio, $\mathscr{A}$	Hydrogen injection temperature, °R	Chamber pressure at injector face, psia	Oxidant-fuel ratio, O/F	Efficiency of characteristic exhaust velocity, percent	Propellant weight flow, lb/sec		Injection velocity, ft/sec		Injector pressure drop, psi		Stability classification
										Hydrogen	Oxygen	Hydrogen	Oxygen	Hydrogen	Oxygen	
P	394	18.5	397	72	2.23	114.1	236.5	4.85	95.07	20.31	98.56	824	89.5	19.89	78.75	Transition
	395	↓	↓	↓	↓	136.2	309	4.90	94.43	26.30	128.8	1001	118	28.18	143.3	↓
	396	↓	↓	↓	↓	118.2	310	4.13	96.87	29.26	120.9	933	111	34.75	107.3	↓
	397	↓	↓	↓	↓	162.5	309	6.22	93.15	22.49	140.0	1043	130	32.21	172.7	↓
Q	306	10.78	201	100	1.9	59.7	319	3.72	97.2	12.83	47.77	151	150	11.74	324	Stable
	307	↓	↓	↓	↓	61.7	316	4.27	96.4	11.61	49.56	147	156	-------	336	Stable
	308	↓	↓	↓	↓	61.5	316	4.69	99.8	10.49	49.18	132	155	-------	329	Transition
	309	↓	↓	↓	↓	64.3	313	5.05	96.3	10.26	51.86	151	163	-------	370	Stable
	310	↓	↓	↓	↓	62.7	312	4.99	94.9	10.41	51.99	140	164	-------	371	↓
	311	↓	↓	↓	↓	65.1	312	5.46	91.9	10.16	55.51	159	175	-------	425	↓
	312	↓	↓	↓	↓	59.8	315	3.65	96.2	13.00	47.48	154	150	-------	299	↓
R	514	10.78	157	72	1.9	110	299	4.82	95.1	10.31	49.72	922	203	100	484	Stable
	515	↓	↓	↓	↓	97	308	3.86	97.6	12.12	46.79	876	191	68.39	459	Transition
	516	↓	↓	↓	↓	128	300	5.36	98.5	9.67	51.83	946	210	72.2	579	Stable
	517	↓	↓	↓	↓	105	285	6.02	94.1	8.59	51.71	759	211	41.8	567	Transition
	518	↓	↓	↓	↓	113	291	5.38	95.6	9.31	50.10	894	205	55.48	528	↓
	519	↓	↓	↓	↓	108	290	5.03	95.2	9.74	48.95	984	201	57.33	505	↓
S	498	9.93	421	100	1.612	72.4	311	4.96	95.1	10.20	50.63	242	108	8.423	197	Transition
	499	↓	↓	↓	↓	69.4	316	3.88	95.6	12.25	47.50	235	102	13.61	170	↓
	500	↓	↓	↓	↓	70.6	299	5.98	91.2	9.08	54.34	208	115	7.617	227	↓
T	383	10.78	397	---	1.9	82.8	303	4.18	95.8	10.39	43.47	409	99	8.85	112	Stable
	384	↓	↓	↓	↓	68.1	308	4.75	90.7	10.18	48.38	206	109	7.93	152	Transition
	385	↓	↓	↓	↓	65.6	307	3.79	91.6	11.73	44.48	189	101	14.20	126	↓
	386	↓	↓	↓	↓	67.4	298	5.77	85.9	9.16	52.84	188	120	11.27	175	↓

U	424	10.78	397	---	1.9	76	309	4.82	100.5	10.07	48.50	317	110	14.01	123	Transition
	425	↓	↓	↓	↓	67	325	3.76	101.4	12.54	47.09	201	107	17.87	107	↓
	426	↓	↓	↓	↓	83.1	296	5.83	96.4	8.89	51.84	363	118	11.66	158	↓
	427	↓	↓	↓	↓	58.9	320	3.31	101.7	13.53	44.73	140	101	20.90	112	Stable
	428	↓	↓	↓	↓	77.0	314	5.22	99.1	9.84	51.37	308	116	12.50	163	Transition
V	429	10.78	397	---	1.9	81	318	4.77	104.0	10.07	48.08	354	109	27.84	159	Transition
	431	↓	↓	↓	↓	74	305	3.81	99.6	11.85	45.16	344	102	16.64	137	Transition
	432	↓	↓	↓	↓	61.5	302	5.99	92.4	9.25	55.41	107	126	9.29	170	Stable
	---	↓	↓	↓	↓	-----	---	----	------	-----	------	----	-----	------	---	---------
	434	↓	↓	↓	↓	77	319	4.28	102.0	11.03	47.26	340	107	26.23	144	Transition
	435	↓	↓	↓	↓	97.6	305	5.19	101.0	9.42	48.91	490	111	18.99	151	Transition
W	441	10.78	397	---	1.9	103	319	4.73	99.5	10.74	50.76	574	115	22.97	173	Transition
	442	↓	↓	↓	↓	95	311	3.79	110.0	11.92	45.19	581	103	21.63	130	↓
	443	↓	↓	↓	↓	120	318	5.67	99.3	9.53	54.01	630	123	15.09	170	↓
	444	↓	↓	↓	↓	101	311	4.25	101.0	11.08	47.10	589	107	19.13	136	↓
	445	↓	↓	↓	↓	122	318	5.18	99.7	10.03	51.99	412	117	15.50	168	↓
X	436	10.78	397	---	1.9	169.8	299	5.55	98.8	9.06	50.24	957	114	14.90	174	Transition
	437	↓	↓	↓	↓	117.6	315	3.87	99.8	12.13	46.92	791	106	24.94	151	↓
	438	↓	↓	↓	↓	188.6	301	6.77	98.9	8.03	54.34	942	123	15.67	201	↓
	439	↓	↓	↓	↓	138.4	320	4.32	98.4	11.56	49.96	906	113	21.52	144	↓
	440	↓	↓	↓	↓	182.3	300	6.19	97.9	8.56	52.98	971	120	16.88	177	↓
Y	392	10.78	397	---	1.9	100	304	4.74	97.8	10.09	47.87	548	109	30.39	145	Transition
	393	↓	↓	↓	↓	93	304	3.77	99.4	11.73	44.70	563	101	37.07	128	↓
	394	↓	↓	↓	↓	106	304	5.76	97.5	8.93	51.43	526	117	23.89	160	↓
	395	↓	↓	↓	↓	93	302	4.26	97.4	10.86	46.31	529	106	33.86	148	↓
	396	↓	↓	↓	↓	103	302	5.22	95.9	9.61	50.14	544	114	26.89	146	↓
	397	↓	↓	↓	↓	100	303	5.22	96.7	9.62	50.20	522	115	29.49	147	↓

TABLE II. - Continued. EXPERIMENTAL DATA

(b) SI units

Combustor configuration	Test	Chamber diameter, cm	Number of injection elements	Element radial distribution, percent	Contraction ratio, ϵ	Hydrogen injection temperature, K	Chamber pressure at injector face, kN/m^2	Oxidant-fuel ratio, O/F	Efficiency of characteristic exhaust velocity, percent	Propellant weight flow, kg/sec		Injection velocity, m/sec		Injector pressure drop, kN/m^2		Stability classification
										Hydrogen	Oxygen	Hydrogen	Oxygen	Hydrogen	Oxygen	
A	292	27.38	397	100	1.9	63.3	2185	4.85	102.0	4.58	22.19	192	33.8	330	924	Stable
	---					----	----	----	-----	----	-----	---	----	---	----	----------
	294					35.2	2385	4.84	97.3	5.24	25.36	42.2	38.7	79.2	1248	Transition
	295					36.3	2247	3.83	93.1	6.09	23.33	57.3	35.7	138	1082	
	296					35.2	2330	5.67	96.1	4.66	26.44	37.8	40.5	67.6	1324	
	297					34.4	2309	6.19	93.5	4.49	27.78	34.4	42.4	73.1	1496	
B	772	25.22	397	100	1.61	35.7	2165	4.47	98.2	4.96	22.16	41.1	33.8	61.1	1041	Transition
	773					34.4	2158	5.43	100.4	4.24	23.00	31.1	35.1	99.3	1082	Stable
	---					----	----	----	-----	----	-----	----	----	----	----	---------
	775					34.7	2151	5.98	100.9	3.95	23.64	29.9	35.9	48.1	1213	Transition
	776					33.1	2158	3.61	99.9	5.65	20.41	37.8	31.1	101.3	958	Stable
C	552	23.24	397	100	1.37	35.9	2116	4.99	89.1	4.71	23.54	44.2	36.6	58.7	1179	Transition
	553					35.9	2096	3.93	90.6	5.42	21.30	51.2	32.9	60.0	972	
	554					35.5	2144	5.53	90.9	4.38	24.19	38.4	37.2	67.3	1344	
	555					34.6	2199	4.34	90.1	5.33	23.11	41.7	35.4	94.6	1109	
	556					34.8	2192	5.70	92.3	4.33	24.70	34.7	37.8	82.9	1517	
D	369	21.21	397	100	1.14	36.4	2048	3.82	88.0	5.13	19.58	71.0	39.3	105	779	Transition
	370					39.6	2041	4.71	90.64	4.45	20.95	87.5	30.8	142	841	
	371					32.5	2165	5.56	87.7	4.37	24.29	44.8	35.6	172	1379	
	372					32.2	2172	4.70	89.21	4.82	22.66	66.4	32.6	226	1082	
	373					32.0	2192	3.67	88.7	5.81	21.34	55.2	30.8	268	1068	

E	262	39.88	397	100	4.34	42.2	2254	3.55	94.2	5.71	20.29	103	33.5	94.4	848	Stable
	---					----	----	----	-----	----	-----	-----	----	-----	----	
	265					38.4	2116	4.75	90.2	4.74	22.53	66.7	35.1	88.5	986	
	266					40.67	2103	3.88	80.7	6.11	23.75	109.4	36.9	139.7	1144	
	269					36.1	2103	3.93	80.2	6.12	24.02	55.5	36.9	133	1213	
	270					36.1	2116	3.97	78.8	6.22	24.68	55.8	38.1	96.2	1206	
F	358	27.38	397	85	1.9	65.6	2061	5.03	99.4	4.35	21.89	210	33.5	247	1041	Transition
	360					58.3	2109	3.24	97.5	6.18	20.04	239	30.8	368	765	Stable
	361					61.7	2061	4.01	97.8	5.13	20.53	225	31.4	321	889	Transition
	362					93.9	2178	6.51	95.9	3.89	25.30	246	39.0	268	1379	
	363					80.6	2048	5.66	96.1	4.04	22.86	240	34.7	263	1103	
	364					65.6	2041	4.61	100.5	4.66	21.46	217	32.6	272	979	
	365					82.2	2041	6.26	99.0	3.79	23.73	227	36.3	256	1179	
G	546	27.38	397	72	1.9	75.6	2199	3.82	109.2	5.56	21.25	278	32.9	449	862	Stable
	547					67.2	2144	3.88	97.2	5.53	21.46	244	33.5	320	993	Transition
	548					78.3	2178	4.95	97.9	4.70	23.25	246	35.9	336	1082	
	549					85.0	2185	5.88	97.4	4.23	24.85	242	38.1	272	1309	
	550					70.6	2172	4.30	96.3	5.26	22.60	240	32.6	345	1020	
	551					81.7	2185	5.66	96.7	4.37	24.76	242	38.4	-----	----	
H	347	27.38	397	60	1.9	67.8	2041	5.16	92.9	4.51	23.28	223	35.4	253	1234	Transition
	348					58.3	2075	4.11	94.1	5.19	21.31	204	32.3	310	979	
	349					100.6	2165	6.82	101.2	3.67	25.01	265	37.4	267	2054	
	350					92.2	2137	6.86	100	3.66	25.09	173	37.2	215	1282	
	351					67.8	2151	4.69	98.7	4.78	22.44	182	33.8	260	1103	
	352					83.9	2165	6.16	99.4	3.99	24.59	183	36.6	235	1213	
	353					71.7	2089	5.29	98.5	4.36	23.08	202	35.1	283	1082	

TABLE II. - Continued. EXPERIMENTAL DATA

(b) Continued. SI units

Combustor configuration	Test	Chamber diameter, cm	Number of injection elements	Element radial distribution, percent	Contraction ratio, $\mathscr{A}$	Hydrogen injection temperature, K	Chamber pressure at injector face, kN/m^2	Oxidant-fuel ratio, O/F	Efficiency of characteristic exhaust velocity, percent	Propellant weight flow, kg/sec		Injection velocity, m/sec		Injector pressure drop, kN/m^2		Stability classification
										Hydrogen	Oxygen	Hydrogen	Oxygen	Hydrogen	Oxygen	
I	478	24.41	397	75.5	1.51	76.0	2130	5.04	96.2	4.46	23.00	225.5	34.3	238.7	1010.7	Transition
	479					70.6	2103	3.75	93.9	5.59	21.26	262.6	31.9	438.2	943.2	
	480					92.3	2151	6.29	96.4	3.89	24.92	243.3	37.4	269.2	1157.6	
	481					72.1	2130	4.39	95.3	4.96	22.17	235.6	33.3	384.5	919.7	
	482					87.2	2151	5.62	95.9	4.21	24.06	246.2	36.1	251.6	1102.5	
	483					81.5	2137	4.93	95.0	4.59	23.02	250.7	34.7	294.1	988.0	
J	484	23.28	397	83.5	1.37	66.5	2104	4.88	93.9	4.51	22.86	196.4	33.6	322.8	936.3	Transition
	485					45.9	2117	3.99	92.3	5.31	22.26	128.9	32.3	239.1	1045.2	
	486					75.1	2137	6.19	97.9	3.77	23.88	187.5	35.6	169.1	1088.7	
	487					62.0	2082	4.41	93.3	4.83	21.90	194.1	32.4	168.5	1008.7	
	488					73.8	2137	5.62	97.2	4.05	23.29	196.7	34.7	268.6	961.8	
	489					57.3	2117	3.89	94.6	5.28	21.35	187.1	31.4	356.7	803.9	
K	414	32.32	397	72	2.63	121.4	2116	4.83	96.22	4.74	23.27	427	34.7	433	1115	Transition
	416					94.3	2137	3.63	98.57	5.82	21.34	397	32.3	497	830	Transition
	417					138.7	2158	5.71	94.29	4.39	26.09	445	38.1	559	------	Stable
	418					137.9	2151	6.01	95.73	4.15	25.26	420	38.1	499	1314	Stable
	419					136.7	2124	6.03	94.83	4.14	25.12	419	38.1	468	1323	Transition
	422					104.9	2117	4.82	95.03	4.80	23.70	372	35.4	526	1111	Stable
	425					97.9	2144	3.79	98.88	5.62	22.28	399	32.3	531	873	Transition
	426					122.1	2172	5.77	97.95	4.21	24.81	373	37.2	540	1160	Stable
	427					155.7	2158	6.19	94.81	4.11	25.70	384	38.7	636	1630	Stable
	428					106.6	2109	5.15	94.40	4.59	24.16	363	35.9	605	1423	Stable

L	240	43.23	397	85	4.77	105.2	2172	5.08	100.4	4.52	22.96	318	35.7	404	1020	Stable
	241					78.9	2123	5.05	95.5	4.65	23.47	243	36.6	274	1199	Transition
	243					86.1	2165	5.93	101.1	4.15	24.61	235	38.7	269	1165	
	244					80.0	2151	4.70	96.4	5.06	23.81	266	37.2	299	1075	
	245					67.2	2151	4.11	93.4	5.76	23.71	246	36.9	352	1151	
	246					74.5	2144	5.72	88.2	4.83	27.62	233	42.7	298	1544	
M	285	47.04	397	72	5.6	147.2	2192	5.28	103.1	4.55	24.61	449	36.3	489	1144	Transition
	286					105.6	2165	4.22	101.9	5.23	22.08	408	34.1	556	1027	
	287					152.2	2089	6.92	101.2	3.81	26.33	452	38.4	487	1372	
	288					133.9	2158	4.84	96.9	4.97	24.06	378	37.2	553	1213	
	295				5.7	126.1	2130	5.08	102.9	4.38	22.27	378	34.1	525	986	Stable
	297					120.6	2137	4.93	100.3	4.61	22.72	397	35.1	483	1041	Transition
	298					105.6	2165	4.02	97.5	5.62	22.56	420	34.1	570	1034	
	299					138.3	2165	5.85	94.2	4.49	26.23	359	39.9	578	1475	
	300					105.6	2151	4.96	92.5	5.07	25.19	362	37.8	543	1227	
N	386	39.88	397	100	1.61	39.1	2165	4.33	95.3	12.65	54.4	-----	32.9	101	948	Transition
	387					41.9	2136	4.46	86.25	13.54	58.9	87.4	37.2	146	2032	
	388					34.4	2296	5.19	98.77	11.42	57.0	41.5	36.5	31	894	
O	375	43.3	397	85	1.9	54.3	2137	4.85	97.28	11.65	56.10	192	34.7	253	836	Transition
	376					52.9	2130	3.94	94.7	13.69	53.95	-----	32.6	267	878	
	377					62.9	2070	6.21	97.84	9.55	57.71	200	36.6	253	930	
	378					44.2	2109	4.58	89.1	12.83	57.8	-----	35.4	160	1008	
	379					57.3	2070	5.62	98.61	10.10	56.20	186	35.0	185	862	
	380					50.1	2082	4.67	94.4	13.37	53.45	-----	32.9	286	769	

TABLE II. - Concluded. EXPERIMENTAL DATA

(b) Concluded. SI units

Combustor configuration	Test	Chamber diameter, cm	Number of injection elements	Element radial distribution, percent	Contraction ratio, $\mathscr{A}$	Hydrogen injection temperature, K	Chamber pressure at injector face, kN/m^2	Oxidant-fuel ratio, O/F	Efficiency of characteristic exhaust velocity, percent	Propellant weight flow, kg/sec		Injection velocity, m/sec		Injector pressure drop, kN/m^2		Stability classification
										Hydrogen	Oxygen	Hydrogen	Oxygen	Hydrogen	Oxygen	
P	394	47.04	397	72	2.23	63.4	1630	4.85	95.07	9.21	44.68	251	27.2	137	542	Transition
	395					75.7	2130	4.90	94.43	11.92	58.39	305	35.9	194	988	
	396					65.7	2137	4.13	96.87	13.27	54.82	284	33.8	239	740	
	397					90.3	2130	6.22	93.15	10.19	34.76	318	39.6	222	1191	
Q	306	27.38	201	100	1.9	33.2	2199	3.72	97.2	5.82	21.67	46.0	45.7	80.9	2234	Stable
	307					34.3	2178	4.27	96.4	5.27	22.48	44.8	47.5	-----	2316	Stable
	308					34.2	2178	4.69	99.8	4.76	22.31	40.2	47.2	-----	2268	Transition
	309					35.7	2158	5.05	96.3	4.65	23.52	46.0	49.7	-----	2551	Stable
	310					34.8	2151	4.99	94.9	4.72	23.58	42.7	49.9	-----	2557	
	311					36.2	2151	5.46	91.9	4.61	25.18	48.5	53.3	-----	2929	
	312					33.2	2172	3.65	96.2	5.89	21.54	46.9	45.7	-----	2061	
R	514	27.38	157	72	1.9	61.1	2061	4.82	95.1	4.68	22.55	281	61.9	689	3337	Stable
	515					53.9	2123	3.86	97.6	5.49	21.22	267	58.2	471	3164	Transition
	516					71.1	2068	5.36	98.5	4.39	23.51	288	64.0	498	3991	Stable
	517					58.3	1965	6.02	94.1	3.89	23.46	231	64.3	288	3909	Transition
	518					62.8	2006	5.38	95.6	4.22	22.73	272	62.5	382	3640	
	519					60.0	1999	5.03	95.2	4.42	22.20	269	61.3	395	3481	
S	498	25.22	421	100	1.612	40.2	2144	4.96	95.1	4.63	22.96	73.8	32.9	58.1	1358	Transition
	499					38.6	2178	3.88	95.6	5.56	21.55	71.6	31.1	93.8	1172	
	500					39.2	2061	5.98	91.2	4.12	24.65	63.4	35.1	52.5	1564	
T	383	27.38	397	---	1.9	29.3	2089	4.18	95.8	4.71	19.72	125	30.2	61	772	Stable
	384					37.8	2123	4.75	90.7	4.62	21.95	63.0	33.2	55	1048	Transition
	385					36.4	2116	3.79	91.6	5.32	20.18	57.6	31	98	869	
	386					37.4	2054	5.77	85.9	4.15	23.97	57.3	36.6	78	1206	

NASA-Langley, 1969 — 33 E-5012

U	424	27.38	397	---	1.9	42.2	2130	4.82	100.5	4.57	21.99	96.6	33.5	97	848	Transition
	425					37.2	2241	3.76	101.4	5.69	21.36	61.2	32.6	123	738	
	426					46.2	2041	5.83	96.4	4.03	23.51	111	35.9	80	1089	
	427					32.7	2206	3.31	101.7	6.14	20.29	42.7	30.8	144	772	Stable
	428					42.8	2165	5.22	99.1	4.46	23.30	93.9	35.4	86	1124	Stable
V	429	27.38	397	---	1.9	45.0	2192	4.77	104.0	4.57	21.81	107.8	33.2	192	1096	Transition
	431					41.1	2103	3.81	99.6	5.37	20.48	104.8	31.1	115	944	Transition
	432					34.2	2082	5.99	92.4	4.19	25.13	32.6	38.4	64	1172	Stable
	---					----	----	----	-----	-----	-----	-----	----	-----	----	Stable
	434					42.8	2199	4.28	102.0	5.00	21.44	104	32.6	181	993	Transition
	435					54.2	2103	5.19	101.0	4.27	22.18	149.3	33.8	131	1041	Transition
W	441	27.38	397	---	1.9	57.2	2199	4.73	99.5	4.87	23.02	174.9	35.0	158	1193	Transition
	442					52.8	2144	3.79	110.0	5.41	20.49	177	31.4	149	896	
	443					66.7	2192	5.67	99.3	4.32	24.49	192	37.5	104	1172	
	444					56.1	2144	4.25	101.0	5.03	21.36	179.5	32.6	132	937	
	445					67.8	2192	5.18	99.7	4.55	23.58	125.6	35.6	107	1158	
X	436	27.38	397	---	1.9	94.3	2061	5.55	98.8	4.11	22.79	292	35	103	1199	Transition
	437					65.3	2172	3.87	99.8	5.50	21.28	241	32.3	172	1041	
	438					104.8	2075	6.77	98.9	3.64	24.65	287	37.5	108	1386	
	439					76.9	2206	4.32	98.4	5.24	22.66	276	34.4	148	993	
	440					101.3	2068	6.19	97.9	3.88	24.03	296	36.6	116	1220	
Y	392	27.38	397	---	1.9	55.5	2096	4.74	97.8	4.57	21.71	167	33.2	209	999	Transition
	393					51.7	2096	3.77	99.4	5.32	20.27	172	31	256	882	
	394					58.9	2096	5.76	97.5	4.05	23.33	160	36	165	1103	
	395					51.7	2082	4.26	97.4	4.93	21.00	161	32.3	233	1020	
	396					57.2	2082	5.22	95.9	4.36	22.74	166	34.7	185	1006	
	397					55.5	2089	5.22	96.7	4.36	22.77	159	35	203	1013	

"The aeronautical and space activities of the United States shall be conducted so as to contribute . . . to the expansion of human knowledge of phenomena in the atmosphere and space. The Administration shall provide for the widest practicable and appropriate dissemination of information concerning its activities and the results thereof."

— NATIONAL AERONAUTICS AND SPACE ACT OF 1958

NASA SCIENTIFIC AND TECHNICAL PUBLICATIONS

TECHNICAL REPORTS: Scientific and technical information considered important, complete, and a lasting contribution to existing knowledge.

TECHNICAL NOTES: Information less broad in scope but nevertheless of importance as a contribution to existing knowledge.

TECHNICAL MEMORANDUMS: Information receiving limited distribution because of preliminary data, security classification, or other reasons.

CONTRACTOR REPORTS: Scientific and technical information generated under a NASA contract or grant and considered an important contribution to existing knowledge.

TECHNICAL TRANSLATIONS: Information published in a foreign language considered to merit NASA distribution in English.

SPECIAL PUBLICATIONS: Information derived from or of value to NASA activities. Publications include conference proceedings, monographs, data compilations, handbooks, sourcebooks, and special bibliographies.

TECHNOLOGY UTILIZATION PUBLICATIONS: Information on technology used by NASA that may be of particular interest in commercial and other non-aerospace applications. Publications include Tech Briefs, Technology Utilization Reports and Notes, and Technology Surveys.

Details on the availability of these publications may be obtained from:

SCIENTIFIC AND TECHNICAL INFORMATION DIVISION

NATIONAL AERONAUTICS AND SPACE ADMINISTRATION

Washington, D.C. 20546